Abstract

Uppsten, M., 2004, *Crystallographic Studies on the Subunits and Holocomplex of Class Ib Ribonucleotide Reductase.* Doctoral dissertation.
ISSN 1401-6249, ISBN 91-576-6491-9

The enzyme ribonucleotide reductase (RNR) is essential in all cellular organisms since it catalyses the conversion of all four ribonucleotides to corresponding deoxyribonucleotides (dNTPs), the building blocks of DNA. To be able to support the cells with appropriate amounts of dNTPs, RNR is highly allosterically regulated. The biologically active form of class I RNR is thought to be composed of two homodimers, R1 and R2. The enzymatic reduction is initiated by an organic free radical generated by a di-iron site located in the smaller R2 subunit. When the radical is needed for reaction initiation it is transported to the active site in the R1 subunit.
This thesis presents structural studies of class Ib RNR from two different pathogenic bacteria.
M. tuberculosis codes for two different R2 subunits of the class Ib RNR, R2F-1 and R2F-2 respectively. The crystal structure of the R2F-2 subunit was determined to 2.2 Å. It is an all helical protein with the di-iron site positioned within a four helix bundle. The di-iron site is in its reduced state. Comparison of the R2F-2 structure with a model of R2F-1 suggests that the important differences are located at the C-terminus.
The three-dimensional structure of the large subunit of the first member of a class Ib RNR, R1E of *S. typhimurium*, was determined in its native form and in complex with four of its allosteric specificity effectors. The enzyme contains a characteristic 10-stranded α/β-barrel with catalytic residues at a finger loop in its centre. The N-terminal domain is about 50 residues shorter in the class Ib enzymes compared to the class Ia enzymes, which explains the absence of the allosteric overall activity.

The crystal structure of the first holocomplex of any RNR was determined to 4Å. The structure of R1E/R2F from *S. typhimurium* reveals a non symmetric interaction between the two subunits. There is clear binding of a polypeptide in the hydrophobic pocket of one R1E monomer. The pocket is known to mediate the interaction between the two subunits and we propose that it is the C-terminus of an interacting R2F subunit that binds in the cleft.

Keywords: protein X-ray crystallography, allosteric effector, active site cysteine, nucleotide, long-rang-electron-transfer, subunit interaction, diiron carboxylate protein, tyrosyl radical

Author's address: Malin Uppsten, Department of Molecular Biology, Swedish University of Agricultural Sciences, S-751 24 Uppsala, Sweden, *email*: malin.uppsten@molbio.slu.se

To my Family

Contents

Appendix

Appendix A

Table of data collection and refinement statistics for the structure mentioned in Paper III, chapter 5.1.

Papers I-IV

This thesis is based on the following papers, which will be referred to by their Roman numerals:

I. **Uppsten, M**., Davis, J. S., Rubin, H., Uhlin, U. (2004) Crystal structure of the biologically active form of Class Ib Ribonucleotide Reductase small Subunit from *Mycobacterium tuberculosis*. *Revision stage for FEBS Letters.*

II. **Uppsten, M**., Färnegårdh, M., Jordan, A., Ramaswamy, S., Uhlin, U. (2003) Expression and preliminary crystallographic studies of R1E, the large subunit of ribonucleotide reductase from *Salmonella typhimurium*. *Acta Crystallographica* D**59**, 1081-1083

III. **Uppsten, M**., Färnegårdh, M., Jordan, A., Eliasson, R., Eklund, H., Uhlin, U. (2003) Structure of the Large Subunit of Class Ib Ribonucleotide Reductase from *Salmonella typhimurium* and its Complexes with Allosteric Effectors. *Journal of Molecular Biology*, **330**, 87-97

IV. **Uppsten, M**., Färnegårdh, M., Domkin, V., Uhlin, U. (2004) The first Crystal Structure of a Class I Ribonucleotide Reductase Holocomplex. *In manuscript.*

Abbreviations

ADP	adenosine diphosphate
ATP	adenosine triphosphate
CDP	cytidine diphosphate
dATP	deoxyadenosine triphosphate
dCTP	deoxycytidine triphosphate
dGTP	deoxyguanosine triphosphate
dNTP	deoxyribonucleotide, any base
dTTP	deoxythymidine triphosphate
DNA	deoxyribonucleic acid
EM	electron microscopy
E. coli	*Escherichia coli*
EPR	electron paramagnetic resonance
GDP	guanosine diphosphate
Mtb	*Mycobacterium tuberculosis*
M. tuberculosis	*Mycobacterium tuberculosis*
NMR	nuclear magnetic resonance
PCET	proton coupled electron transfer
rmsd	root mean square deviation
R1	Large subunit of Class I RNR
R2	Small subunit of Class I RNR
R1E	Large subunit of Class Ib RNR
R2F	Small subunit of Class Ib RNR
R2F-2	One of the two small subunits of Class Ib RNR present in Mtb.
RNR	ribonucleotide reductase
UDP	uridine diphosphate

1. Introduction

During all ages humans have been exploring both their outer and inner surroundings to answer questions about life and to find clues about their existence. Until not that long ago research was limited to what was visible to the human eye. As the technical development proceeds we are more and more focusing on events and particles that we are not able to visualise without means of technical help, such as a microscope or a telescope. An image of the object we want to study is always of great help in trying to understand its nature.

The specific functions of biological macromolecules, like proteins, are completely dependent on their three-dimensional structures. Methods that enable us to determine the shapes and atomic arrangements of proteins are therefore very useful tools in the process of mapping all the components of different organisms. Intrinsic knowledge about the functions of an increasing number of proteins allows us to design drugs against unwanted events in our own cells, such as different diseases.

There are currently three different methods applicable for structure determination of proteins, electron microscopy, nuclear magnetic resonance (NMR) and X-ray crystallography. Electron microscopy can be used to visualise the overall shape of big molecular complexes but the resolution limit is still too low to be useful for studying the details of protein structures. In NMR the molecular structure is determined from a liquid sample, which is probably the most natural environment for most biological macromolecules. The limitation with this method lies in the number of atoms in the object molecule, and for this reason the majority of proteins are too big for NMR.

X-ray crystallography is the most common method for structure determination of proteins and it is based on the principle of diffraction. If one single protein molecule is put in an X-ray beam the electrons in the molecule will scatter the X-ray photons. When millions of molecules arranged in a periodic manner, like in a crystal, are exposed to monochromatic X-rays, the scattered photons leaving the crystal will interfere with each other. The scattered X-rays are enhanced in some directions and diminished in others. The photons are collected by a photosensitive detector and a diffraction pattern is generated. Every atom in the crystal contributes to the properties of every diffraction spot in the pattern. Finding the relationship between the arrangement of the atoms in the crystal and the diffraction pattern is the computational heart of X-ray crystallography. The intensities of the diffraction spots are proportional to the amplitudes of the diffracted X-rays but the phases of the waves are lost in the experiment. The main obstacle in X-ray crystallography is to determine the relative phases of the diffracted rays and it is referred to as the phase problem.

X-ray crystallography has been used in this work to study one particular enzyme. Enzymes are protein molecules that specialise in making different chemical reactions go faster. Without enzymes the existence of life as we know it today

would not even begin. Ribonucleotide reductase (RNR) is part of the DNA production and it is an indispensable enzyme for all cells. The biologically active RNR is composed of one small and one large subunit. They have different functions and must cooperate for a successful result. The objective of this work is to gain functional knowledge of ribonucleotide reductase by studying its three-dimensional structure.

The first chapter in this thesis gives a general introduction to the enzyme ribonucleotide reductase and it is followed by a short methodological part. The structural results are presented in three different chapters: structure of the small RNR subunit from *Mycobacterium tuberculosis*, structure of the large subunit from *Salmonella typhimurium*, structure of the complex between the small and large subunits from *S. typhimurium*.

2. Ribonucleotide reductase

2.1 Background

All cells and many viruses store their genetic code as DNA, deoxyribonucleic acid. The building blocks that combine to form these cellular blueprints are the deoxyribonucleotides and they are produced by the reduction of the corresponding ribonucleotide. The reduction is catalysed by the enzyme ribonucleotide reductase. A schematic picture of the reaction is presented in Figure 2.1. Ribonucleotide reductase (RNR) is thus an indispensable enzyme for all cells since it catalyses the biosynthesis of the precursors necessary for both synthesis and repair of DNA. There is no alternative pathway for *de novo* synthesis of deoxyribonucleotides and this makes RNR crucial for cell progression in all living organisms (Thelander and Reichard,1979, Reichard,1993, Reichard,1997).

Figure 2.1 The reduction catalysed by ribonucleotide reductase.

In the early 1950s when Reichard with co-workers discovered this reaction they had a hard time trying to convince the scientific world that an enzyme was able to perform a reaction that organic chemists by that time could not manage in one step (Reichard and Rutberg,1960). It was not until the 1970s that it was revealed that RNR utilizes an organic free radical, an unpaired electron, to initiate the reaction. This was an astonishing discovery and RNR was the first enzyme to be assigned the ability to generate, store and use an organic free radical for its reaction (Ehrenberg and Reichard,1972, Reichard and Ehrenberg,1983).

2.2 Different classes of RNR

Depending of the availability of cofactors and oxygen, three main types of radical-generation mechanisms have evolved. They define three classes of ribonucleotide reductases (Reichard,1993, Reichard,1997). There is little sequence similarity among the classes but they share a radical-based reaction mechanism and the enzymes are all allosterically regulated (Stubbe,2000). This thesis will focus on the class I ribonucleotide reductase and for more information on the class II and III enzymes the interested reader is referred to the wide collection of review publications on the subject (Sjöberg,1997, Jordan and Reichard,1998, Eklund, et al.,2001).

The initial studies of ribonucleotide reductase were performed on the aerobic *E. coli* RNR, which was addressed as the prototype for class I RNRs. After the discovery of a variant of the class I reductases it was further divided into subclasses a and b based on sequence homologies and overall allosteric regulation pattern (Jordan, et al.,1994a, Jordan, et al.,1996b). The class Ia enzymes are present in practically all eukaryotes (except Euglena), several viruses and a few bacteria (Torrents, et al.,2002) while the class Ib enzymes have only been found in prokaryotes (Jordan, et al.,1994a, Yang, et al.,1994, Fraser and Venter.,1995, Jordan, et al.,1996b, Scotti, et al.,1996).

Class I RNRs are oxygen-dependent enzymes and are composed of two types of subunits, α and β. The active enzyme is believed to be a tetrameric $\alpha_2\beta_2$-complex (Sjöberg,1997). A schematic picture of the holo enzyme is shown in Figure 2.2. The α subunit is more commonly referred to in dimeric form (α_2) as R1. Each α monomer carries the substrate binding active site and is in charge of the allosteric regulation (Thelander and Reichard,1979). The β subunit is called R2 in its dimeric form and it contains the binding site for the metal centre which generates the radical necessary for the enzymatic reaction (Larsson and Sjöberg,1986, Larsson, et al.,1988).

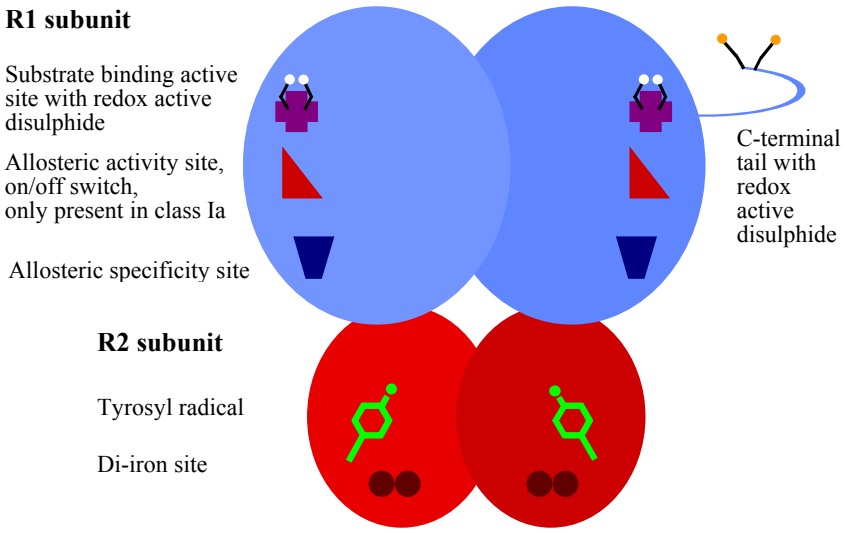

Figure 2.2 Schematic picture of the class I ribonucleotide reductase. The larger R1 subunit on top and the smaller radical generating R2 subunit at the bottom.

2.3 R2 - the heart of RNR

R2 is the smaller one of the two subunits building up the biologically active RNR holoenzyme. Each monomer is composed by approximately 300-400 amino acid residues and has mainly a helical structure. A number of R2 structures from different organisms have been solved by X-ray crystallography. They all share a very similar fold which makes the dimer look like a heart (Figure 2.3) (Nordlund, et al.,1990, Kauppi, et al.,1996, Eriksson, et al.,1998, Huque,2001, Voegtli, et al.,2001, Högbom, et al.,2002, Högbom, et al.,2004). The R2 structure discussed in this thesis is the class Ib R2 from *M. tuberculosis*, called R2F-2 (Paper I).

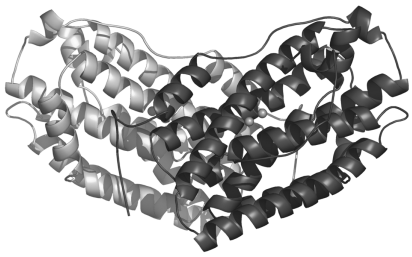

Figure 2.3 Structure of the R2F-2 from *Mycobacterium tuberculosis* (Paper I).

The key element in the catalysis of ribonucleotide reductase is the organic free radical generated and stored in R2. The radical is generated by a di-iron site hidden away in a four helix-bundle within the R2 monomer. Prior to radical generation, the two irons are in their reduced, ferrous state. Upon oxidation an oxygen bridge is formed between them and the generated organic free radical settles on a conserved tyrosine residue close to the two irons. This is also where the radical is stored until it is needed for reaction initiation (Sjöberg and Gräslund,1977, Sjöberg and Reichard,1977, Larsson and Sjöberg,1986, Nordlund, et al.,1990).

The reaction performed in R2 to produce the organic free radical can be written as:

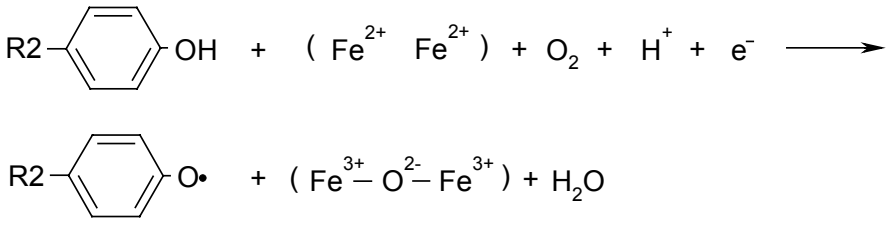

Numerous crystallographic studies have been done in attempts to characterise the iron centre and to understand the mechanism of the radical generation. So far, the R2 from *E. coli* is the one that has been most thoroughly examined. As a result, three different states of the iron centre have been described by X-ray crystallography: the *apo* form, without any iron bound; the *reduced,* diferrous form; and the *met* form, with diferric irons but without radical (Nordlund et al., 1990, Åberg et al., 1993, Logan et al., 1996). The *active* form, where the irons are in the diferric state and the radical is resting on a tyrosine residue has also been structurally described by a combination of X-ray and EPR crystallography (Högbom, et al.,2003). These structures in combination with additional structural investigations, spectroscopic experiments and theoretical calculations have led to proposals for the mechanisms of oxygen activation and radical generation (Andersson, et al.,1999, Assarsson, et al.,2001, Högbom, et al.,2001, Siegbahn,2003, Stubbe,2003).

2.4 R1 – the hand of RNR

The R1 subunit is approximately twice the size of R2, about 700 amino acid residues per monomer. Only two R1 structures of the class I enzymes have so far been determined (Uhlin and Eklund,1994), (Paper III). The R1 monomer is often compared to a hand with the N-terminal part represented by the fingers and the active site in the palm of the hand. The main dimer interaction contains two helices from each monomer that form a four helix bundle between the monomers. (Uhlin and Eklund,1994) (Figure 2.4).

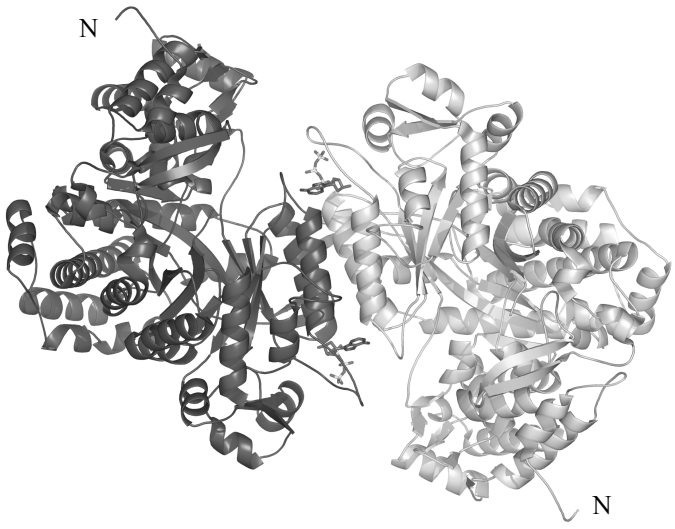

Figure 2.4 Structure of the R1E dimer from *Salmonella typhimurium* (Paper II and III). The two monomers are colored in dark and light gray respectively with the effector dATP bound at the specificity sites.

The active site in R1 is located in the middle of the α/β barrel, in the palm of the hand analogy (Uhlin and Eklund,1994). The reduction catalysed by RNR might look simple at first glance but is in fact no trivial task. A proposed mechanism for the enzymatic reduction has been developed for the class I enzymes (Figure 2.5). It is based on experimental data from several biochemical studies, active site mutants as well as advanced EPR (electron paramagnetic resonance) methods (Mao, et al.,1992a, Stubbe and van der Donk,1998).

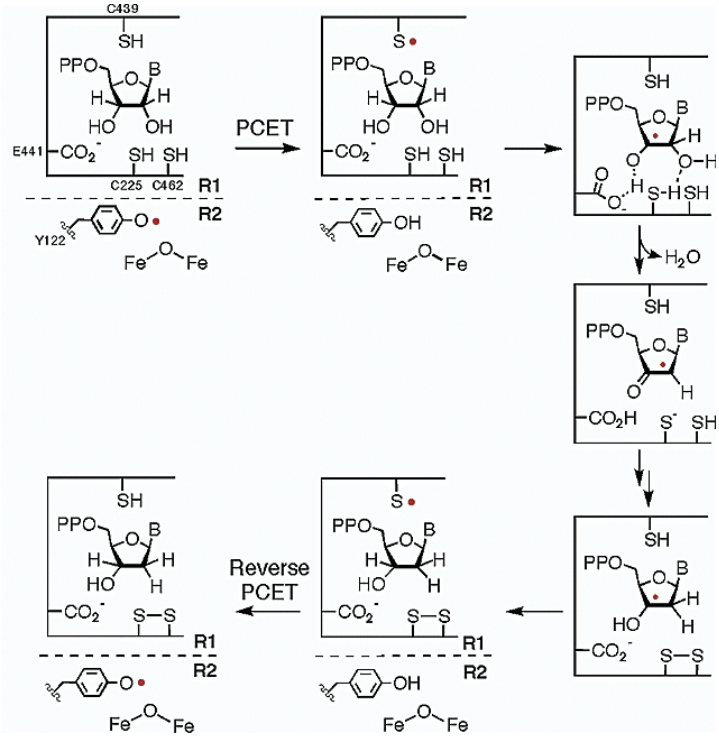

Figure 2.5 The reaction mechanism performed by the bigger R1 subunit in class I ribonucleotide reductase, as described in Ge et al., 2003 (*E. coli* numbering).

The reaction mechanism involves five conserved amino acid residues in the active site, an asparagine, a glutamate and three cysteines. The asparagine and the glutamate are involved in substrate binding and form hydrogen bonds to the 2' and 3' oxygens of the substrate ribose. When the substrate is bound the radical is delivered from R2 to the active site in R1 where it ends up on one of the conserved cysteine residues. From here the radical attacks the substrate (Mao, et al.,1992b). The reducing power needed in the reaction is supplied by a fully conserved redox active cysteine pair in the active site. Once the reduction is performed the disulphide is re-reduced by a second cysteine pair in the C-terminus of R1 which is thought to swing into the active site for this purpose (Figure 2.2) (Åberg, et al.,1989, Mao, et al.,1992a, Mao, et al.,1992b, Uhlin and Eklund,1994). The C-

terminal disulphide in turn gets reduced by the external electron donors of the system. Thus, the C-terminal tail of the R1 protein acts as a shuttle transporting electrons from the electron donors to the catalytic site. In class Ia the external electrons are received from the two ubiquitous small redox proteins glutaredoxin and thioredoxin (Holmgren,1989) whereas the class Ib systems utilises a specific nrdH redoxin (Jordan, et al.,1997).

Like many enzymes at metabolic key points, RNR is highly allosterically regulated. Since RNR catalyses the reduction of all four ribonucleotides, a precise regulation mechanism is crucial to ensure the production of appropriate amounts of all four deoxyribonucleotides. Apart from the active site where the substrate reduction takes place, R1 has a binding site for effectors specifying which substrate is to be reduced, the allosteric specificity site (Figure 2.2). Regulation of the substrate specificity is similar in all classes of ribonucleotide reductase. Binding of ATP or dATP to the specificity site induces reduction of UDP and CDP. Binding of dTTP and dGTP induces the reduction of GDP and ADP respectively (Brown and Reichard,1969b, Thelander and Reichard,1979, Reichard,1993, Eliasson, et al.,1996). The specificity sites are located across the dimer interface at both ends of the four helix bundle created by two helices from each subunit (Figure 2.4). When an effector is bound at this site it interacts with three loops, loops 1-3. It is believed that conformational changes in these loops, together with the interaction with R2, facilitate the substrate preference at the active site (Eriksson, et al.,1997).

Apart from the specificity site, the class Ia has an additional allosteric site called the overall activity site. This site acts as the on/off switch of the enzyme (Figure 2.2). Bound dATP acts as an inhibitor whereas ATP activates class Ia RNR (Brown, et al.,1969, Thelander and Reichard,1979). The overall activity site is located in the N-terminal part of R1 (Eriksson, et al.,1997) and since the class Ib subunit is about 50 residues shorter than class Ia R1 in this region, the allosteric activity site is absent (Eliasson, et al.,1996). A third allosteric site, called the H-site has been suggested to be present in the mammalian system (Scott, et al.,2001, Kashlan, et al.,2002).

A more detailed structural description of the big subunit is presented in Paper III. The class Ib subunit, R1E, from *S. typhimurium* RNR is described. Moreover, the allosteric regulation is discussed from a structural point of view.

2.5 The holocomplex

Neither of the two subunits are able to perform the enzymatic reaction by itself. Both of them carry components necessary for the reduction. The bigger R1 subunit harbours the substrate binding active site and the smaller R2 is crucial for the delivery of the organic free radical. In some way the radical has to be delivered from R2 to R1. When R1 and its active site are ready to perform the reduction, a signal is sent to R2, which releases the radical. The radical is transferred to the active site in R1 from where it attacks the substrate (Sjöberg,1994). After the

substrate reduction, the radical is thought to be recovered to the tyrosine in R2 and further stored until the next turnover (Ge, et al.,2003).

The radical transfer is thought to happen through a long-range hydrogen bonded pathway where several residues from each subunit are involved (Figure 2.6). Several of them have been identified by mutational studies and structurally characterised, but some parts of the hydrogen bonded chain are still missing (Larsson and Sjöberg,1986, Åberg, et al.,1989, Nordlund, et al.,1990, Climent, et al.,1992, Mao, et al.,1992b, Rova, et al.,1995, Ekberg, et al.,1996, Persson, et al.,1996, Ekberg, et al.,1998, Rova, et al.,1999). How the signalling system works between the subunits and how the radical is transferred between R2 and R1 is not yet known.

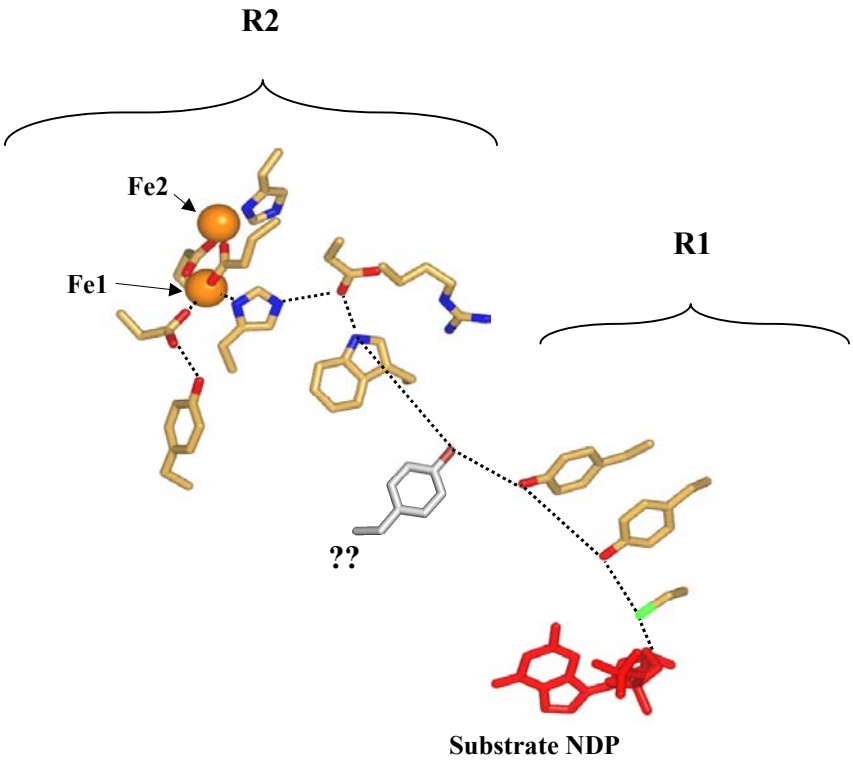

Figure 2.6 The proposed radical path from the diiron site in R2 to the active site and substrate in R1.

For a successful enzymatic reduction to take place R1 and R2 have to interact with each other and form a holocomplex. The two homodimers are stable in solution and it has been shown by sucrose gradient experiments that they form a complex composed of one R1 dimer and one R2 dimer (Brown and Reichard,1969a, Thelander,1973). The only thing known about the interaction between the two subunits is that the C-terminus of R2 binds to a hydrophobic cleft on R1 and that

this binding is essential for an active enzyme. The interaction is species specific and if the C-terminus of R2 is truncated the interaction as well as the enzymatic activity is diminished (Cohen, et al.,1986, Dutia, et al.,1986, Sjöberg, et al.,1987, Climent, et al.,1991, Cosentino, et al.,1991). If the hydrophobic interaction described above is the only interaction between R1 and R2 or if an additional contact is necessary for radical delivery has not yet been established.

The first crystal structure of a class I RNR holocomplex, containing both subunits, is presented in Paper IV. Structural aspects on the interaction between the two subunits are discussed.

2.6 Class Ib RNR

The division of class I RNRs into two subclasses (a and b) was suggested when it was discovered that some bacteria code for two different class I enzymes. To distinguish between the two subclasses the subunits of class Ia are depicted R1 and R2 and the class Ib subunits are named R1E and R2F after their respective genes, *nrdE* and *nrdF* (Jordan, et al.,1994a, Jordan, et al.,1994b). It has been shown that in organisms where both subclasses are present the *nrdAB* genes code for the essential class Ia enzyme whereas the *nrdEF* operon is only weakly transcribed. The *nrdEF* genes are not essential to these cells either during aerobic nor anaerobic growth (Jordan, et al.,1996a, Jordan, et al.,1996b). The reason for organisms to have two, or even three functional ribonucleotide reductase systems is not known.

Class Ib ribonucleotide reductases have been found in widely different prokaryotes including *Salmonella typhimurium, Lactococcus lactis, Bacillus subtilis, Mycoplasma genitalium*, and *Mycobacterium tuberculosis*, as well as in aerobically grown *E. coli* (Jordan, et al.,1994a, Yang, et al.,1994, Fraser and Venter.,1995, Jordan, et al.,1996b, Scotti, et al.,1996). In the cases known, the class Ib RNRs are not the active class of enzymes reducing ribonucleotides in the cells, with the only exception so far being *M. tuberculosis* RNR (Yang, et al.,1994) (Paper I).

Class Ib RNR is closely related to the class Ia enzymes. They differ mainly in allosteric regulation. As mentioned earlier, the N-terminal part of the class Ib R1E is about 50 residues shorter than in the class Ia R1 subunit and as a consequence the allosteric activity site is absent in class Ib RNR (Eliasson, et al.,1996). This means that Ib RNRs lack general negative control of ribonucleotide reduction that turns off the enzyme when dNTPs accumulate. Also, class II enzymes do not have this type of control, which therefore does not exist in most prokaryotes. Eukaryotic cells on the other hand employ class Ia enzymes and therefore have a more sophisticated ribonucleotide reductase which protects them from the possible toxic and mutagenic effects that may arise from the overproduction of dATP and other dNTPs (Kunz,1988).

A quite distinct difference between the *nrdAB* and the *nrdEF* operons is that the Ib operon code for an additional protein, NrdI of unknown function and often also

for a specific external electron donor NrdH. NrdH-redoxin has thioredoxin-like properties but a glutaredoxin-like amino acid sequence and it is a specific reductant of the R1E/R2F system (Jordan, et al.,1996a, Jordan, et al.,1996b, Jordan, et al.,1997, Stehr, et al.,2001).

The fact that RNR alone is responsible for supplying the cells with DNA building blocks makes it a very interesting target for antiproliferating drugs. Class Ib appears to be the biologically active form of *M. tuberculosis* and possibly also in other pathogens. In view of that, the structures presented in this thesis should be important guides for further studies of attractive drug targets within this family.

3. Method

3.1 Phasing

All structures presented in this thesis have been determined by X-ray crystallography. The phasing method used is molecular replacement and the special strategy employed in the structure determination of the R1E/R2F complex is further described in section 6.7.1, (Paper IV).

3.2 Crystallisation

A prerequisite for X-ray crystallography to be successful is of course good diffracting crystals. Obtaining suitable crystals is the least understood, and often the most difficult component of protein crystallography. The crystallisation method used in all the projects presented in this thesis is the vapour diffusion technique (Figure 3.1). A droplet of pure protein solution, typically 2 µl, is put on a cover slip and mixed with an equal amount of a crystallising solution (usually buffer, salts and precipitants). The cover slip with the protein drop is placed as a lid for a small well, typically 1 ml, and sealed with silicon grease. After the well is sealed, water vaporises from the drop to establish equilibrium between the drop and the solution in the well. In the process, the concentrations in the drop increase. With some skill and a lot of luck the protein concentration reaches supersaturation and the crystal nucleation occurs at, or close to the point of equilibrium. As a crystal nucleus is formed the protein molecules overcome an energy barrier and they become more stable in the ordered crystal than in solution.

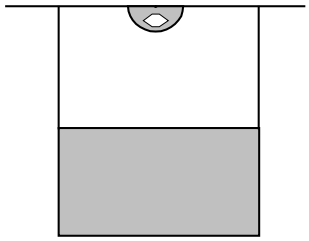

Figure 3.1 Crystallisation setup in the hanging drop, vapor diffusion technique. When the setup is successful a crystal grows in the drop.

The nucleation event is often very critical. If too many nuclei are formed simultaneously the protein will form a precipitate, which is useless for diffraction experiments. This problem is usually overcome by lowering the protein or/and the precipitant concentration. If, on the contrary, no nucleation takes place it is possible to introduce nuclei to the system. The easiest and most common way is by transferring nuclei from another crystallisation drop with the help of, for example, a cat whisker. A protein crystal, or a drop solution containing crystals, can be touched with the whisker. By consecutively streaking the whisker through the new crystallisation drop, nuclei can be transferred (Bergfors,1999).

Streak seeding can also be used as a tool to improve the diffraction quality of crystals or in an attempt to alter the crystal space group. The space group change

phenomenon was obtained unintentionally both when crystallising R1E as well as the R1E/R2F complex from *S. typhimurium* (Paper II-IV).

4. R2F-2 from *Mycobacterium tuberculosis* (Paper I)

4.1 Introduction

In all known cases, class Ib RNRs are not expressed and utilised for nucleotide reduction under normal conditions, with the only exception so far being *Mycobacterium tuberculosis* RNR. The RNR enzyme from this pathogen has attracted attention because tuberculosis remains a major global disease infecting one-third of the world population and killing more than 2 million people each year (WHO,2003). The resistance against known drugs is becoming an increasing problem and since RNR is a potential drug target is it important to investigate the features of this particular enzyme.

Surprisingly it was found that the *M. tuberculosis* (Mtb) genome codes for two separate small class Ib RNR proteins. The two proteins, R2F-1 and R2F-2, are composed of 322 and 324 amino acid residues respectively and have 71% amino acid identity (Yang, et al.,1997). Both are postulated to contain an iron-radical site like other class I R2 proteins (Yang, et al.,1997) and enzymatic investigations revealed that R2F-2 form the recombinant active enzyme together with R1E. Also R2F-1 was able to form a holocomplex with R1E in vivo, but only if it was present in concentrations higher than R2F-2.

4.2 Overall structure of R2F-2

The R2F-2 from Mtb is an all helical protein. The two monomers are combined to form a heart shaped dimer similar to the previously known R2 structures (Nordlund, et al.,1990, Kauppi, et al.,1996, Eriksson, et al.,1998, Högbom, et al.,2002). Each R2F-2 monomer is made up of eleven helices of which eight, αA-H, form a bundle and three shorter helices, α1, α2 and α4, are peripherally located in the structure (Figure 4.1).

Of the 324 amino acids in the R2F-2 sequence, 288 have been traced in the electron density maps of the best defined subunit. The first 8-9 residues at the N-termini are invisible as well as the last 28-38 residues with variations between the molecules in the asymmetric unit. The C-terminus known to be crucial in the interaction to R1E is not visible in the electron density maps.

As expected from the earlier known R2 structures, Mtb R2F-2 is most similar to the structures of *S. typhimurium* R2F (rmsd 1.04Å for 283Cα) and *C. ammoniagenes* R2F (rmsd 0.86Å for 285 Cα). These two proteins also belong to the class Ib enzymes and have a sequence identity of 77% and 66% respectively to Mtb R2F-2.

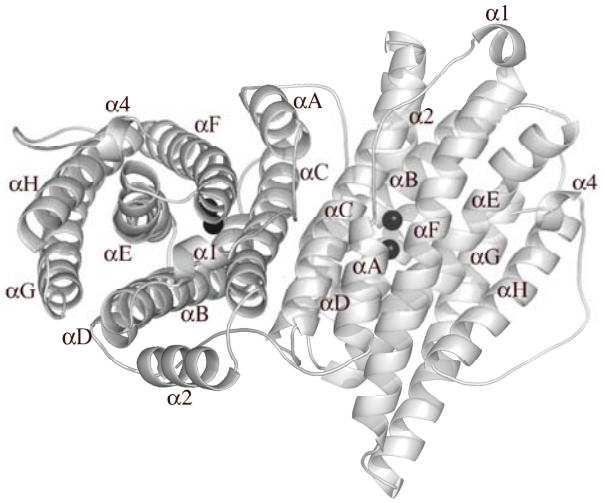

Figure 4.1 Structure of the R2F dimer from *Mycobacterium tuberculosis.* The two monomers are oriented roughly perpendicular to each other.

4.3 The metal site

The R2F-2 dimer has two equivalent dinuclear iron centres. Each centre is well buried within a four helix bundle. The two irons are ligated by amino acid residues from all four helices, Asp72 from αB, Glu103 and His106 from αC, Glu163 from αE, and Glu197 and His200 from αF (Figure 4.2). Hence there are four carboxy ligands and two histidine ligands and in addition also a water molecule. Glutamate 103 and 197 are both bridging the two irons and Glu163 ligates bidentate to Fe2. The water molecule binds only to Fe2 making it 6-coordinate with a square-pyramidal shape as opposed to Fe1, which has 4 ligands creating a tetraheadral coordination. This situation is identical in the structure of the reduced *S. typhimurium* R2F while in the reduced *C. ammoniagenes* R2F, the water molecule ligating Fe2 is absent.

Where both the ferrous and the ferric states of the iron site have been studied from the same class Ib R2F, two glutamic acids change their conformations between the states. In the ferric state, the side chain of the glutamate corresponding to Glu163 in Mtb moves away from the iron making room for the second glutamate, Glu197 in Mtb. The side chain of this residue moves and ligates only Fe2 in the oxidised state.

No crystal structure of Mtb R2F-2 has been obtained where the metal site is oxidised. Several datasets have been collected, but all of them were found to be reduced, probably by X-ray radiation. Combination of initial images from different crystals show only minor differences compared to full datasets. The use of glycerol as a cryo protectant was shown to promote reduction of the *S. typhimurium* R2 diiron site, and PEG400 had to be used instead (Eriksson, et

al.,1998). In the case with Mtb R2F-2 however, the metal centre was found to be reduced both with glycerol and PEG400 as cryo protectant.

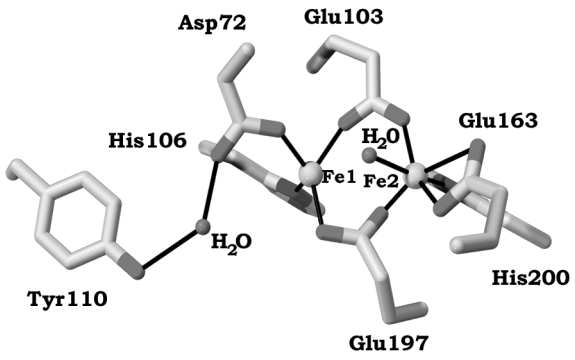

Figure 4.2 Crystallographic structure of the reduced diiron site in Mtb R2F-2. The six iron ligating amino acids and the tyrosine residue on which the radical is known to settle before it is needed for reaction.

In order to determine the oxidation state of the diiron centre in different crystals microspectrophotometry was used. According to earlier characterisation of the R2F-2 protein, the tyrosyl radical gives a prominent peak at 408 nm. The dominant features of the diferric cluster in R2F-2 are absorption bands at 325, 370 nm as well as very weak bands at 480 and 620 nm (Liu, et al.,1998). Upon reduction of the di-iron site the radical peak is absent and the iron bands are diminished. Several spectra were collected between 320 and 560 nm both on freshly prepared crystals and on crystals previously exposed to X-rays. Attempts were also made to collect spectra on crystals soaked in 20mM hydrogen peroxide in order to generate the tyrosyl radical in the crystal by the so-called shunt-pathway (Sahlin, et al.,1990). The unique radical peak could not be found in any spectra indicating the absence of a tyrosyl radical in the crystals. Unfortunately no characteristic absorption band could be observed in any spectra and it was not possible to assign the redox state of any crystal. This is most likely because the diferric absorption bands are broad and there are thus only minor differences in absorption between the two oxidation states in the absence of the radical species.

4.4 The tyrosyl radical

The radical harbouring tyrosine in Mtb R2F-2, Tyr110, is about 6.8Å from the closest iron atom. The tyrosine residue is in its protonated state and within hydrogen bonding distance (2.7Å) to a water molecule, which in turn forms a

hydrogen bond to Asp72. The distance between the phenolic oxygen of Tyr110 and the closest carboxylate oxygen of Asp72 is 4.5-4.8Å.

The distant tyrosine and the bridging water molecule has been suggested to be a common feature among the class Ib proteins (Liu, et al.,1998, Högbom, et al.,2002).

4.5 The αE helix

The αE is one of the helices in the four-helix bundle providing ligands to the metal centre. In all solved R2 structures the hydrogen-bonding pattern of the αE helix is distorted. This is due to an extra amino acid causing the formation of a π-type turn in the middle of the helix.

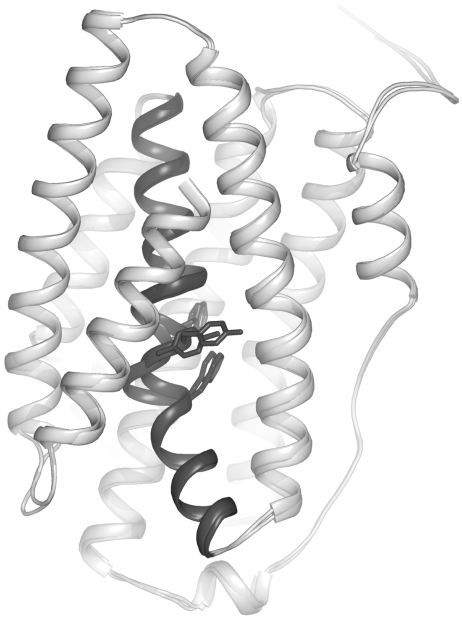

Figure 4.3 Conformational differences in helix E. Superposition of the Mtb R2F-2 monomer with the R2F monomer from *S. typhimurium*, both with reduced diiron sites. The most pronounced movement is displayed by a tyrosine in αE (Y168 in Mtb, Y163 in *S. typhimurium*), which in the Mtb structure stretches out to the surface of the protein.

The distortion differs among earlier determined R2 structures (Kauppi, et al.,1996, Logan, et al.,1996, Eriksson, et al.,1998, Högbom, et al.,2002) and there seems to be a tendency for two different conformations among the class Ib structures. The most pronounced movement is displayed by a tyrosine in αE (Y168 in Mtb, Y163 in *S. typhimurium*). One of the preferred αE conformations is seen in the structure

of Mtb R2F-2 (Figure 4.3), where the diiron centre is reduced. It has the same conformation as αE in *S. typhimurium* when the diiron centre is oxidised (rmsd 0.24 for 29 amino acids in αE). In the structure of *S. typhimurium* where the irons are reduced, however, the conformation of αE is very similar to the one seen in the structures of *C. ammoniagenes* regardless of the redox state of the metal centre. R2F from *S. typhimurium* is so far the only R2 showing alternative conformations of αE in the wild type protein appearing to be dependent on the redox state of the diiron centre. The movement of αE can however not be associated with a certain redox state of the metal centre and the mobility of the helix has not been possible to explain by data currently available.

In the Mtb R2F-2 structure there are indications of movements in the αE helix. Difference Fourier maps (Fo-Fc) reveal that αE has more than one conformation and when combinations of initial images from different crystals were made, the matter became even more apparent.

4.6 R2F-1

A three-dimensional molecular model for Mtb protein R2F-1 was built, based on the structure of Mtb R2F-2. All the iron ligands and mechanism-related residues are conserved in both proteins as well as the residues postulated to be involved in the hydrogen bonded pathway for the radical. The hydrophobic pocket where the tyrosyl radical is stored is almost identical in the two proteins. The only difference being Met189 in R2F-2 located about 7Å from the radical storing tyrosine, which is replaced by a leucine in R2F-1.

4.7 Conclusion

The R2F-2 from *M. tuberculosis* is an all helical protein with a very similar fold as the class Ib R2F subunits from *S. typhimurium* and *C. ammoniagenes*. The distant radical-harbouring tyrosine residue with a bridging water molecule, which previously has been suggested to be common features among the class Ib R2F proteins, is true also for Mtb R2F-2.

The structural similarity between Mtb R2F-1 and R2F-2 indicate that both of them could in principle serve as a functional small subunit. The discrepancy between the two R2s lies instead in the C-terminal sequence, which is crucial for the interaction with the larger R1E subunit.

5. R1E from *Salmonella typhimurium* and its allosteric effectors (Papers II and III)

5.1 Introduction

Like many organisms *S. typhimurium* codes for both class Ia and Ib types of ribonucleotide reductases. The genes *nrdE* and *nrdF* from *S. typhimurium* were the first class Ib RNR to be sequenced and cloned. When it was discovered that they differed from the former known class I enzymes, the *S. typhimurium* enzyme became the prototype for the class Ib RNRs (Jordan, et al.,1994b). The two subunits were named R1E and R2F after their respective genes. The structure presented here is the R1E from *S. typhimurium* with and without allosteric specificity effectors. Crystal structures of R1E without effector and in complex with dATP, dCTP and dTTP have previously been published (Uppsten, et al.,2003). Data collection and refinement statistics for the structure of R1E in complex with dGTP can be found in Appendix A.

5.2 Crystallisation (Paper II)

R1E from *S. typhimurium* crystallised in three different space groups, two orthorhombic and one tetragonal space group. The initial crystal form $C222_1$, has unit cell dimensions of a= 133 Å, b=148 Å, and c= 291 Å. One dataset to 3.2 Å could be collected. The space group of the second crystal form was $P2_12_12_1$. Unfortunately the data was significantly anisotropic with diffraction to around 2.5 Å resolution along one axis but only to 3.5 Å resolution along the other. The cell parameters of the $P2_12_12_1$ crystals are a=59 Å, b=158 Å, and c=170 Å.

The best ordered crystal belongs to the spacegroup $P4_32_12$ and could only be obtained after streak seeding from drops containing $C222_1$ crystals of R1E. The $P4_32_12$ crystals diffracted as best to 2.8Å and have cell dimensions a=99 Å, b=99 Å, and c=290 Å. They contain only one R1E monomer per asymmetric unit and have a solvent content of 73 %.

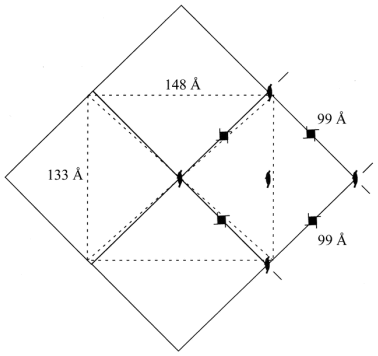

Figure 5.1 Relationship between the orthorhombic $C222_1$ (dotted lines) and tetragonal $p4_32_12$ lattices in the R1E crystals. The lengths of the a and b axes are marked.

When comparing the cell axes of the $P4_32_12$ crystals and the $C222_1$ crystals the following can be stated. The lengths of the a=b cell axes (99Å) of the $P4_32_12$ space group corresponds to a $C222_1$ subgroup with unit cell axes a=b=140Å showing an

increase of the a axis of 7Å and a decrease of the b axis of 8Å. The c axes in the two space groups are approximately of the same length. Thus, streak seeding with material from $C222_1$ crystals resulted in new crystals with super group symmetry. Figure 5.1 illustrates the relationship between the $C222_1$ and the $P4_32_12$ space groups.

5.3 Structure of the salmonella hand, R1E (Paper III)

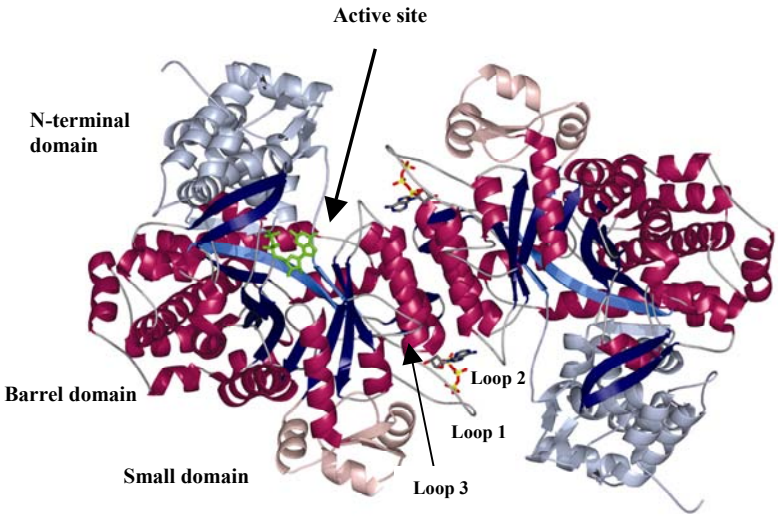

Figure 5.2 Structure of the R1E dimer from *S. typhimurium*. The allosteric specificity sites, here shown with dATP bound, are located at both ends of the four helix bundle created by two helices from each monomer. The location of the substrate GDP (in green) has been modeled in from the *E. coli* structure.

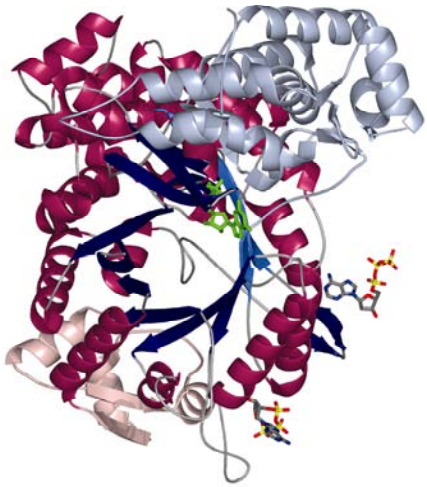

Figure 5.3 The *S. typhimurium* R1E monomer looking down the ten-stranded α/β-barrel to the active site. The substrate GDP (in green) has been modeled in from the *E. coli* R1 structure. The allosteric specificity sites are shown with dATP bound.

5.3.1 Monomer structure

The R1E monomer is composed of three different domains. One large 10-stranded α/β-barrel of about 480 residues, a small α-β domain that packs at the bottom of the barrel, and an N-terminal domain (Figures 5.2 and 5.3). The shape of the monomer can be compared to a hand where N-terminal domain represents the fingers and the active site lies in the palm of the hand, in the 10-stranded barrel (Uhlin and Eklund,1994).

The barrel includes two halves of parallel β-stands. The half-barrels are arranged antiparallel to each other forming an elliptical barrel. The redox active cysteines necessary for the enzymatic reduction are positioned on neighbouring, antiparallel strands. One feature of the barrel is a loop, called the finger loop, inserted in the centre of the barrel with the important residues Cys, Glu and Asn on its tip.

Figure 5.4 Comparison of R1E (in black) with the superimposed *E. coli* R1 (in light gray). The biggest differences is at the N-terminal part at the top.

The characteristic 10-stranded RNR-barrel was first shown in the *E. coli* R1 structure (Uhlin and Eklund,1994) and later seen in related structures of other classes of RNR and in pyruvate formate lyase (Becker, et al.,1999, Eklund and Fontecave,1999, Logan, et al.,1999, Larsson, et al.,2001, Sintchak, et al.,2002). A comparison between the overall structures of R1E and *E. coli* R1 reveals very similar lengths and conformations of strands and helices in the first barrel half, whereas in the second half-barrel, there are some differences (Figure 5.4). The N-terminal domain is most dissimilar between the two enzymes and the first 50 residues of R1 have no counterpart in R1E. In R1, this is where the overall allosteric activity effector binding site is located, and the lack of such a site is one of the characteristics of the class Ib enzymes (Eliasson, et al.,1996). The remaining part of the domain has the same fold as the R1-domain but generally differs in details much more than other parts of the structure.

5.3.2 The dimer

The dimer interaction area in R1E is created by a crystallographic two-fold axis (Figure 5.2). It is dominated by two helices from the barrel of each subunit forming a four-helix bundle. The contact area between the helices from each

subunit is dominated by hydrophobic interactions except for the surface that is directed against the side of the dimer where the active site is located, which contains charged and polar residues. The subunit interaction area in R1E is extended compared to *E. coli* R1 due to a four residue longer connection between the finger-loop and the second half-barrel. This extended loop covers the four-helix bundle at the subunit interface on one side of the dimer.

5.3.3 The active site

Cys388 is located in the centre of the barrel at the tip of the barrel loop (Figure 5.5). This residue is considered to be transiently transformed to a thiyl radical that removes a hydrogen from the 3'-carbon of the substrate initiating the catalytic transformation of the substrate to a 2'-deoxyribonucleotide (Stubbe, et al.,2001). Glu390 and Asn386 are implicated in substrate binding, and are also positioned on the finger loop. The redox active cysteines, 178 and 415, are located on adjacent strands of the barrel, and form a disulfide in the oxidized form. The active site in R1E is very similar to the one in *E. coli* R1 and all the mechanism-related residues are conserved and have equivalent positions.

Crystal structures of R1E where the redox-active thiol/disulphide couple are in reduced and oxidized form have been determined (Figure 5.5). Cys415 in the reduced structure moves away from the active site by about 5 Å and the distance between the two cysteine sulphur atoms is 6.5 Å in the reduced form. The side chain of the next residue, Asn416, also moves significantly (3.4 Å).

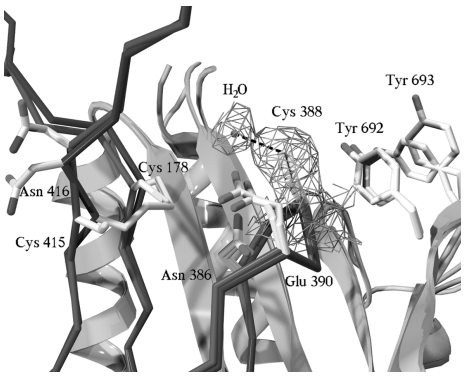

Figure 5.5 The active site in R1E with redox active cysteine residues in their oxidised and reduced forms. The differences are mainly located to C415 and the neighbouring N416. C388 has some extra density in all oxidised structures, interpreted as a water molecule. Y693 in the radical transfer chain has two conformations in most R1E structures, which are shown in the figure.

Close to the radical forming Cys388 in R1E, two tyrosine residues (Tyr692 and Tyr693) have been implemented in the radical transfer chain from R2F to the active site in R1E. Tyr692 seems to have a stable position but the tyrosine most distant from Cys388 (Tyr693) has different conformations in different datasets. In the dTTP dataset this side chain appears to have two conformations.

Although substrates have been present in many of the crystallisation solutions, no substrate binding can be detected in any of the structures.

5.3.4 A plausible binding site for the R2F C-terminus

The R1E subunit is unable to perform the enzymatic reduction without an organic free radical supplied by the smaller R2F subunit. R2F docks to R1E with the help of its C-terminus (Cohen, et al.,1986, Dutia, et al.,1986, Sjöberg, et al.,1987, Cosentino, et al.,1991). In the R1E structure there is a hydrophobic cleft with Phe297 on α10 and Phe351 on αD in its bottom (Figure 5.6). This hydrophobic pocket appears to be a suitable binding site for the C-terminal of R2F and that it can be involved in protein-protein interactions is demonstrated by the crystal packing of R1E where it mediates one of the crystal contacts. The N-terminus of each R1E monomer reaches into the hydrophobic cleft of a neighbouring monomer.

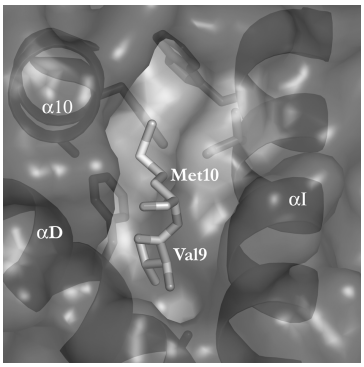

Figure 5.6 The N-terminal Val9 and Met10 of one R1E monomer binds in the hydrophobic cleft of another R1E monomer in the crystal packing. The hydrophobic amino acid residues shown in the pocket are F297 and A300 on α10, F351 and A355 on αD and W684 and I681 on αI.

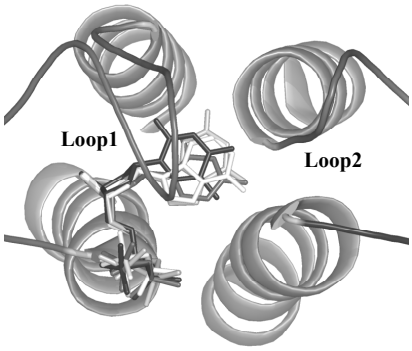

Figure 5.7 Binding of four of the effectors to the allosteric specificity site. The base is inserted into a hydrophobic pocket at the end of the four-helix bundle created by two helices from each monomer. dATP is shown in white, dGTP in light grey, dCTP in medium grey and dTTP in dark grey.

5.3.5 The effector-binding site

Allosteric regulation in class Ib RNR is achieved solely by binding of nucleotide triphosphates to the substrate specificity sites. Five different structures of R1E have been solved. Four of the structures are complexes between R1E and its allosteric specificity effectors, dATP, dCTP, dTTP and dGTP. Binding of dATP promotes the reduction of CDP and UDP. dCTP is a very weak effector for GDP reduction, dTTP gives the best fit for the guanine base at the substrate binding site, and binding of dGTP to the specificity site induces the substrate binding site to attract ADP (Eliasson, et al.,1996). In addition to the four complex structures, the native structure of R1E was solved without any effector bound to the allosteric site.

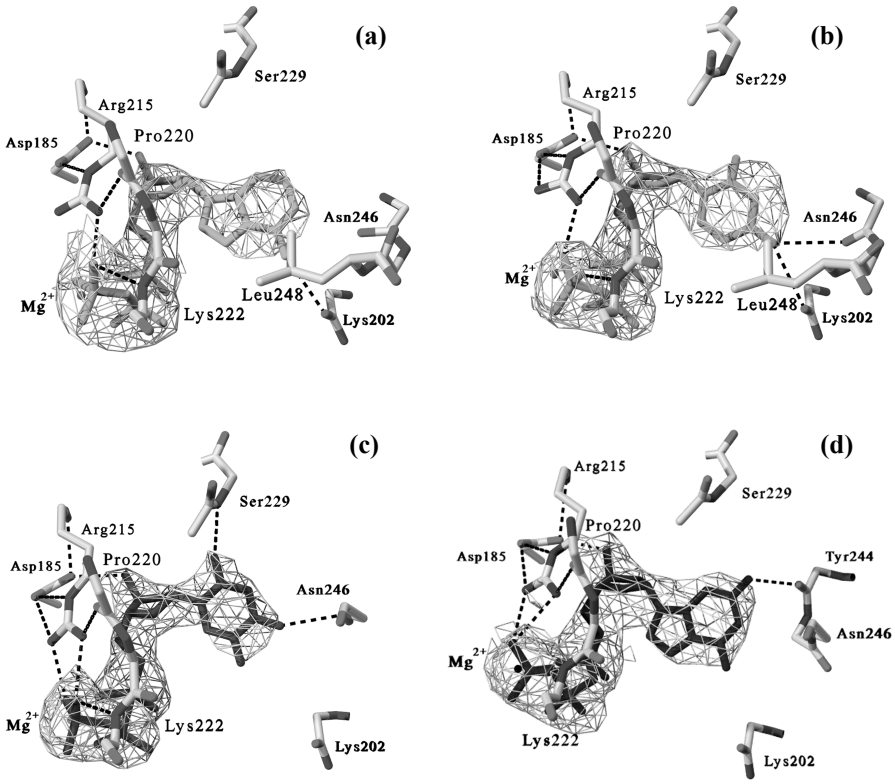

Figure 5.8 Binding of effectors to the allosteric specificity site. **(a)** dATP, **(b)** dCTP, **(c)** dTTP, **(d)** dGTP: Specific interactions made by each of the effectors to R1E. Residues making similar interactions with the effectors are not shown. Final $2F_o$-F_c maps are contoured at 1σ where the effector and magnesium ions have been excluded from the refinement.

The allosteric specificity sites are located across the dimer interface in R1E at a site about 14 Å from one of the active sites in the dimer. The allosteric effect is thought to be mediated by the different conformation of three loops in the R1E structure, loops 1-3 (Figure 5.2). The effector-binding site is formed between the two subunits at the dimer interface, where residues 201-203 and 244-248 (loop 2) come from one subunit and 185-190 and 215-230 (loop 1) from the other (Figure 5.7). The phosphate groups are positioned predominantly by loop1, and the base lies between the monomers coming closer to the active site of the second monomer. The base is positioned in a hydrophobic pocket with Met187 on one side of the base ring and Ile221 stacking to the base on the other side. In the complex structures with dATP (Figure 5.8a) and dCTP (Figure 5.8b) Leu248 stacks with the base on the same side as Ile221 but in the dTTP and the dGTP complexes (Figure 5.8c and 5.8d respectively), loop2 is flexible and the position of Leu248 cannot be determined. Beside hydrophobic interactions, dCTP only has

weak hydrogen bonds from N4 to the carbonyl oxygens of residues Asn246 and Lys202. The base of dTTP forms a hydrogen bond from O2 to the main-chain nitrogen of Ser229 and O4 to the main-chain nitrogen of Asn246. The purine bases of dGTP and dATP have very similar positions in the two effector complexes. From the adenine base in dATP, N6 forms a hydrogen bond to the carbonyl oxygen of residue 202. The base of dGTP forms a hydrogen bond from N2 to the carbonyl oxygen of residue 244.
For all four nucleotides, 3´-OH of the deoxyribose forms a hydrogen bond to Asp185. The side chain of Tyr244 is close to the 2´-carbon, which explains the strong preference for deoxyribonucleotides since 2´-OH of a ribonucleotide would cause steric hindrance.

The phosphate site is located at the N-terminus of a helix αA and the α-phosphate forms a weak hydrogen bond to the main chain nitrogen of residue 187 in the first turn of the helix. There are positively charged residues close to all three phosphates of the effector nucleotides. The magnesium ion is coordinated by all three phosphates and not coordinated by any protein ligand.

The substrate specificity site in R1E has several similarities with that of R1 in *E. coli.* Binding of the phosphates of the effector appears to be more conserved than the hydrophobic pocket positioning the base.

5.3.6 Comparison among the different effector complexes

Loop1 is ordered all R1E structures. Loop 2 in R1E is ordered in the dCTP and dATP complexes but disordered with dTTP, dGTP and in the structure without any effector. Loop 3, which may indirectly influence the conformation of the two other loops, is ordered in the dATP complex and the structure in the absence of effector. There are only minor overall changes between the structure in the absence of effector and those with effectors, the largest differences are about 1 Å. A summary of the loop conformations in the different effector complexes is listed in Table 1.

Table 1. Influence of allosteric specificity effectors on *S. typhimurium* R1E.

Effector	None	ATP	dATP	dCTP	dGTP	dTTP
Preferred substrate	(CDP) (UDP)	CDP, UDP	CDP, UDP	(GDP)	ADP	GDP
Structure resolution (Å)	3.0	-	3.2	3.0	3.0	2.8
Visibility of loops						
Loop 1	yes	-	yes	yes	yes	yes
Loop 2	no	-	yes	yes	no	no
Loop 3	yes	-	yes	no	no	no

It was suggested from the first complexes of *E. coli* R1 with allosteric effectors (Eriksson, et al.,1997) that the regulation of substrate specificity occurs indirectly

by the influence of the effectors on loops that can interact with the base of the substrate. Particularly, loop2 had a position between the effector site and the substrate site that could influence the base site. Further studies of RNRs from other classes have strengthened this view (Larsson, et al.,2001, Sintchak, et al.,2002). Furthermore, studies of the class III RNR with effectors established that large conformational changes in loop 2, were induced by effector binding (Larsson, et al.,2001).

5.4 Conclusion

The overall structure of *S. typhimurium* R1E contains three major domains. One N-terminal domain, one 10-stranded α/β-barrel and one small domain. The N-terminal domain is approximately 50 residues shorter than in the class Ia enzymes, which explains the lack of allosteric overall activity site present in class Ia. The 10-stranded α/β-barrel as well as the small domain are similar to corresponding domains in the class Ia *E. coli* R1. The *E. coli* R1 and the *S. typhimurium* R1E sequences are 20% identical in a structural alignment and the rms difference for 565 Cα- atoms is 1.6 Å.

It appears that a detailed picture of how the allosteric regulation occurs is not possible to obtain in the absence of the R2F subunit since all the loops are probably influenced by substrate binding and formation of an R1E/R2F complex.

6. The RNR holocomplex from *Salmonella typhimurium* (Paper IV)

A number of crystal structures of R1 and R2 from class I RNR have been determined during the last years. Presented here is the first structure of a class I holocomplex containing both subunits giving structural insight into subunit interaction at a resolution of 4 Ångströms.

6.1 Background

6.1.1 The crucial contact

The biologically active class I RNR holoenzyme is thought to be composed of one R1 homodimer and one R2 homodimer. Suggestions have also been made that the major active form of the mammalian system is a $R1_6R2_2$ complex (Scott, et al.,2001, Kashlan, et al.,2002). The key interaction between the two subunits in all cases is the binding of the C-terminal tail of R2 in a hydrophobic cleft in R1 (Cohen, et al.,1986, Dutia, et al.,1986, Sjöberg, et al.,1987, Climent, et al.,1991, Cosentino, et al.,1991, Uhlin and Eklund,1994). Close to the C-terminus of R2 is a conserved tyrosine residue (Y304 in *S. typhimurium* R2F), which has been proposed to be part of the radical transfer between the radical generating diiron centre in R2 and cysteine residue at the active site in R1 (Cys388 in *S. typhimurium*) (Rova, et al.,1999).

When the structure of *E. coli* R1 was determined it was crystallised together with a C-terminal peptide of *E. coli* R2 (Uhlin and Eklund,1994). The last eight residues of the peptide was found to bind in a hydrophobic cleft of R1. It was suggested that the observed binding is the crucial interaction between the subunits in the biologically active system. The interaction revealed by this crystal structure imposes a binding directionality of the R1 cleft, which will be referred to later.

The hydrophobic pocket has also been shown to be good for interactions between R1E molecules. In the R1E structure it mediated one of the crystal contacts. (Paper III).

6.1.2 Radical transport

The control of the transport of the free radical is a key element in the catalysis. A detailed mechanism for radical generation has been proposed (Andersson, et al.,1999, Assarsson, et al.,2001, Högbom, et al.,2001, Siegbahn,2003, Stubbe,2003) but the subsequent transfer to R1 is not as well studied. Series of mutagenesis studies have identified several residues essential for a long-range radical transfer pathway between the subunits (Figure 6.1) (Larsson and Sjöberg,1986, Åberg, et al.,1989, Nordlund, et al.,1990, Climent, et al.,1992, Mao, et al.,1992b, Rova, et al.,1995, Ekberg, et al.,1996, Persson, et al.,1996, Ekberg, et al.,1998, Rova, et al.,1999). Parts of the pathway have been suggested to be a proton-coupled electron transfer (Ekberg, et al.,1998, Siegbahn, et al.,1998, Stubbe, et al.,2003).

In *S. typhimurium* R2F, the transfer includes Tyr105, iron ligands Asp67 and His101, Glu191, Trp31 and a tyrosine at the C-terminus. The C-terminal tyrosine, Tyr304, was shown to be crucial for radical transfer (Climent, et al.,1992). This residue has however not been possible to position in any R2 structure so far. The C-terminal tail of R2 is flexible in all solved R2 structures up to date.

In R1E, the residue presumed closest to R2F to accept the radical is Tyr693, close to the active site. Tyr693 stacks with a second tyrosine located on the same beta strand, Tyr692, (Ekberg, et al.,1996, Rova, et al.,1999). Their hydroxyl oxygens form a hydrogen-bonded path to the sulphur atom of Cys388 from where the radical attacks the substrate (Uhlin and Eklund,1994, Licht, et al.,1996, Sjöberg,1997).

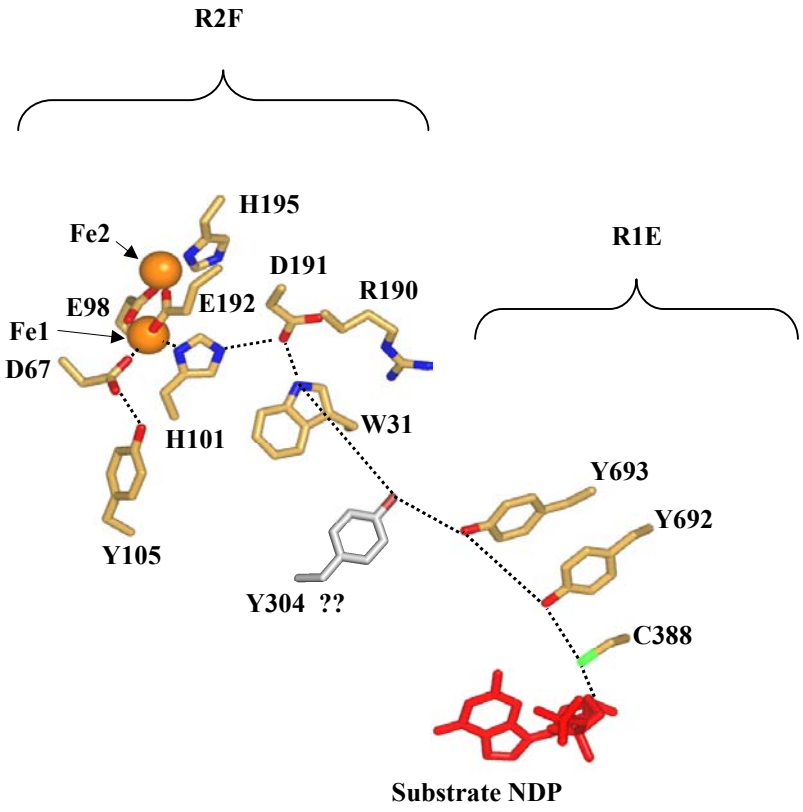

Figure 6.1 Proposed hydrogen bonded radical transfer pathway in *S. typhimurium*. The radical is generated by the diiron site in R2F (top left) and transferred to a cysteine residue in the active site of R1E (bottom right). Tyrosine 304 is positioned close to the C-terminus of R2F and has not been structurally characterised.

6.2 Crystal packing and overall structure

6.2.1 R1E structure

The two R1E monomers in the asymmetric unit are equally well defined in the electron density, 689 of the 714 amino acid residues in the sequence have been traced. The first 10-11 residues as well as the last 15 are not visible in the electron density maps. All crystallisation trials were performed with both substrate and specificity effector present in the crystallisation drops. Unfortunately, in all of the solved complex structures, the disulphides at the active site are oxidized and no substrate seems to be bound. The allosteric effector dGTP however, is bound to the specificity site in all structures.

Three loops are involved in allosteric regulation and possible formation of the holoenzyme, loop 1, 2 and 3. In the R1E/R2F complex structure loop 1 is ordered in both R1E monomers, whereas loop 2 seems to be flexible in both. Loop 3 is clearly defined in only one of the monomers. The conformation is the same as when the R1E subunit was crystallized separately, both without any effector and in complex with dATP (Uppsten, et al.,2003). There is no apparent structural reason why only one of the monomers should have an ordered loop 3. The resolution of the complex data is however not high enough for a detailed study on the structural basis of allosteric regulation.

6.2.2 R2F structure

The two R2F monomers in the asymmetric unit are not equally well defined in the electron density. Only one of the monomers interacts with R1E dimers in the crystal packing, and the electron density for this monomer is much better defined. The second monomer interacts exclusively with its dimer partner, which probably makes it less stabilised in the crystal packing. Of the 319 amino acid residues in the R2F sequence, 283 could be traced in the electron density. The first 5 N-terminal residues are flexible as well as the essential C-terminal tail of R2F where 31-33 residues are missing. The tyrosine residue (Y304) essential for the radical transfer between R1E and R2F is also located in this flexible part of R2F, and therefore, cannot either be seen in the structure.

The more defined R2F monomer has density for the iron-centre while the other R2F monomer has not. Nothing can be said about the redox-state of the R2F protein or the iron-ligands at this low resolution.

6.3 Subunit interactions

In the crystal both tetrameric and hexameric formations of subunits can be observed due to the crystallographic symmetry. When the structure of the *E. coli* R1 was solved it was found to crystallise in trimers of dimers (Uhlin and Eklund,1994). The hexameric interactions observed in the *E. coli* R1 crystal packing does however not have any resemblance with the interactions between different R1E homodimers in the R1E/R2F complex crystals.

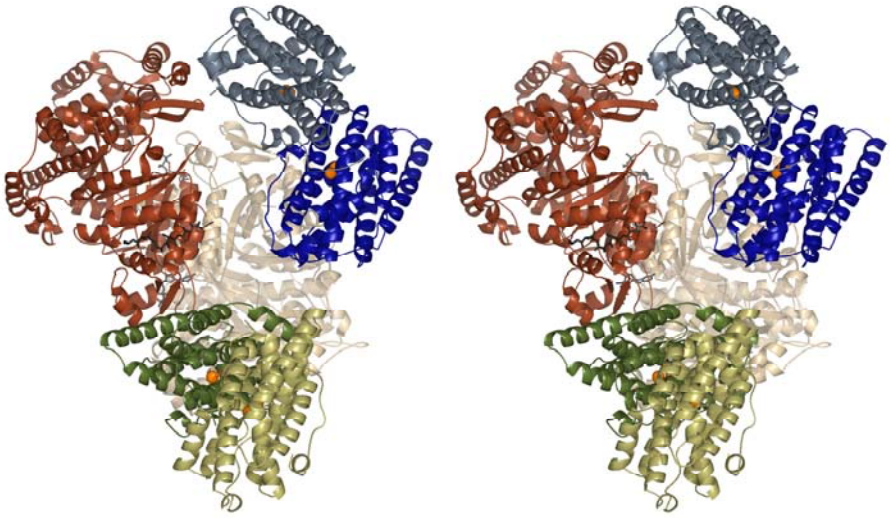

Figure 6.2 Stereo image of the packing interactions between the S-shaped dimer of R1E (in pink and red) and two dimers of R2F, at the top right (interaction A, R2F in blue) and bottom left (interaction B, R2F in green).

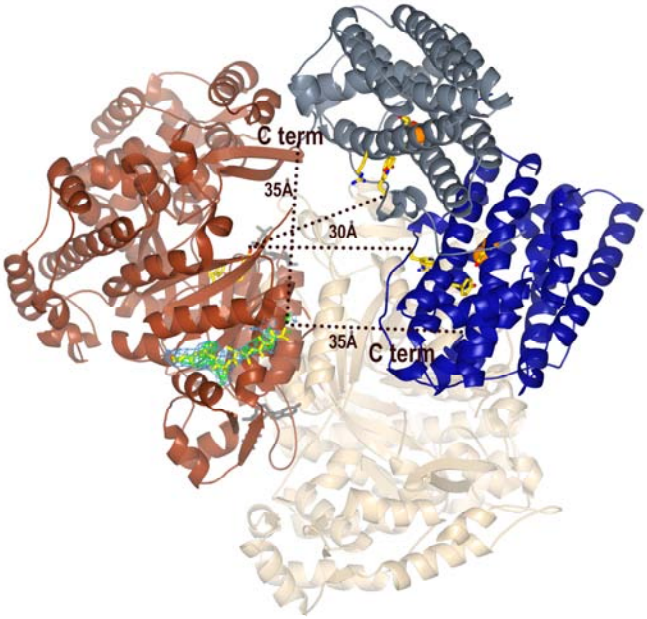

Figure 6.3 Interaction A in the same view as in Figure 6.2. The R2F interacts only with the N-terminal domain on R1E (top of picture). Active site residues, effectors and the octa-peptide bound to one of the R1E monomers are shown as stick representations.

In the R1E/R2F complex crystal each R1E dimer interacts with two R2F dimers, one in the same asymmetric unit, interaction A, and one in the neighbouring asymmetric unit, interaction B (Figure 6.2). Interaction A involves only one monomer from each R1E and R2F dimer (Figure 6.3). Only non-specific interactions are formed between the top of one heart-lobe on R2F and the R1E β-hairpin close to the N-terminal domain of the subunit. The buried surface area in the interaction is approximately 360 $Å^2$, which is less than 2% of the total surface area of the R2F dimer. This is a very weak interaction.

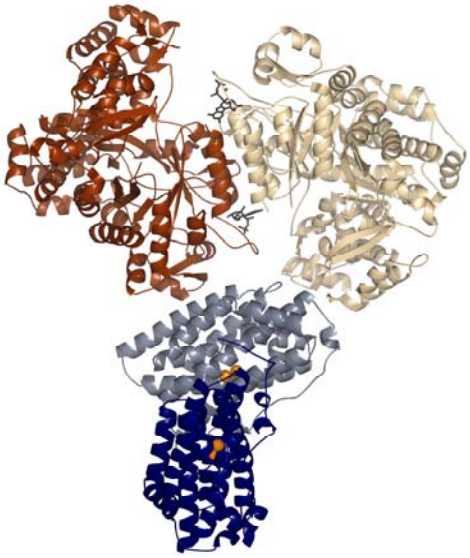

Figure 6.4 Interaction B in a different view compared to 6.2. The allosteric effectors dGTP, bound on both sides on the dimer interface are shown as grey sticks.

In interaction B, one R2F monomer interacts with both R1E monomers (Figure 6.4). The two homodimers are aligned in one plane. It is the same R2F monomer that mediates both interaction A and B, leaving the second R2F monomer without contact to any R1E subunit. In interaction B there are both hydrogen bonding interactions and hydrophobic interactions. The interaction area of 670 $Å^2$ corresponds to 3% of the total surface area of R2F.

6.3.1 A plausible R1E-R2F contact

In the structure of the R1E/R2F complex there is clear electron density for a polypeptide tail in the hydrophobic cleft in one of the R1E monomers in the asymmetric unit (Figure 6.5). The hydrophobic cleft in R1E is located in a groove between three alpha helices, α10, αD, and αI. The bottom of the cleft contains three stacking aromatic amino acid residues: Phe297 on α10, Phe351on αD and Trp684 on αI. Other hydrophobic residues at the site are Ala300, Ala355 and Ile681. The positive electron density in the hydrophobic cleft is elongated and continuous. Judged from the density, Arg685 is suggested to bind to the carboxyl end of R2F as does Lys584 in *E. coli* (Uhlin and Eklund,1994). There is clear density for a side chain at the end of the cleft, which is likely to correspond to the side chain of R2F Trp317 located three residues from the C-terminal end of the polypeptide chain. Unfortunately the limited resolution of the data does not allow tracing of the peptide sequence, therefore an octapeptide of alanines was built in the positive density. It is not likely that anything else added in the crystallisation drops could be represented by this kind of electron density.

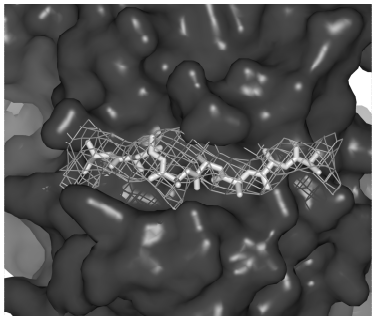

Figure 6.5. A surface representation of the occupied hydrophobic cleft on R1E. with the bound peptide. An octa-peptide has been modelled into the pocket, shown in the picture as sticks. Omit map contoured at 1σ

The crystal packing allows the possibility of four alternative peptide termini to interact with the hydrophobic cleft of the R1E monomer. One possibility is the C-terminus from the same R1E monomer but considering the more hydrophilic C-terminal sequence of R1E, it seems unlikely that the C-terminus of R1E would have a greater affinity for the hydrophobic pocket than would the C-terminus of R2F. Moreover the C-terminus of R1E contains a redox active cysteine pair which need to be flexible to be able to deliver electrons to the active site disulphide.

Three different R2F monomers in the crystal packing are close enough to the peptide binding cleft in R1E, to be able to stretch their C-termini into this binding site. Two of them belong to the R2F dimer, forming the A interaction with the R1E monomer (Figure 6.3). Either of the termini from the R2F dimer are possible candidates for binding in the R1E pocket. The density for the R2F monomer actually interacting with R1E is best defined as earlier discussed, but there are 31 residues missing in its C-terminus. In the second R2F monomer, 33 amino acid residues have not been traced in the electron density maps. The distance between the last traceable residue and the opening of the R1E binding site is approximately 35Å for both monomers.

The third R2F monomer theoretically able to bind to the hydrophobic cleft of R1E in the crystal is located in a different asymmetric unit and does not have any crystal contact with the R1E of interest. The only possibility for this R2F C-terminus to interact with the hydrophobic pocket, is with a reversed binding directionality compared to the *E. coli* case. It does not seem probable that this R2F C-terminus would be the binding one when there are two other R2F monomers within closer distance and with possibility to retain the binding directionality of the cleft.

6.4 Radical transfer

The C-terminus of R2 has not been structurally characterised in any structure so far. This is also the case in the *S. typhimurium* R1E/R2F complex structure, apart from the residues occupying the hydrophobic cleft. With these eight residues included, there are 31 amino acid residues missing in this part of the structure. The

last structurally positioned residue known to be involved in the radical transfer pathway within R2F is Trp31 (W48 *E. coli* numbering), located on the subunit surface at the tip of the heart lobe close to the dimer interface.

In the holocomplex structure of *S. typhimurium,* the closest distance is about 30 Å between any active site R1E Tyr693 to any R2F Trp31. This distance has been measured from the R1E monomer having an occupied hydrophobic cleft, to both of the A-interacting R2F monomers (Figure 6.3). Only one of the R2F monomers is in contact with R1E but Trp31 in both monomers are equally close to the active site. From both Trp31 in the R2F monomers to the second R1E active site, the distance is considerable longer, approximately 50Å.

6.5 Comparison of holocomplex: *S. typhimurium* structure versus the *E. coli* model

In connection to the determination of the *E. coli* R1 structure, a theoretical model of the holocomplex was made (Figure 6.6a) (Uhlin and Eklund,1994). The model was build based on: position of conserved residues on R2 close to the R1 active site; shape complementarities and the theory that two homodimers have a common twofold axis.

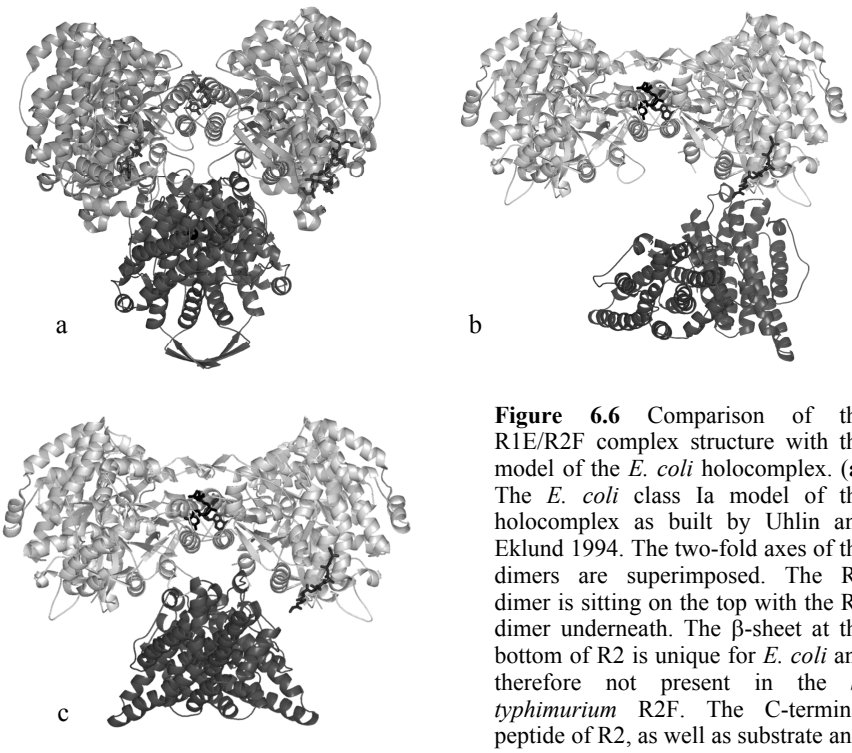

Figure 6.6 Comparison of the R1E/R2F complex structure with the model of the *E. coli* holocomplex. (**a)** The *E. coli* class Ia model of the holocomplex as built by Uhlin and Eklund 1994. The two-fold axes of the dimers are superimposed. The R1 dimer is sitting on the top with the R2 dimer underneath. The β-sheet at the bottom of R2 is unique for *E. coli* and therefore not present in the *S. typhimurium* R2F. The C-terminal peptide of R2, as well as substrate and allosteric effectors are shown as stick models. (**b)** The R1E/R2F complex in interaction A, with the R1E dimer in the same view as in the *E. coli* model. Shown as stick models in R1E are: The effector dGTP between the helices in the four-helix bundle at the dimer axis and the peptide in the hydrophobic cleft. **(c)** The same complex and view as in b, but the R2F dimer has been "flipped" to mimic the *E. coli* model in **(a)**.

In the model the distance between the tryptophan on the surface of R2 (*E. coli* W48, *S. typhimurium* W31) and the closest active site tyrosine (Y731 in *E. coli*, Y693 in *S. typhimurium*) is 25 Å. There is no alternative way of docking the two subunits that would place these two residues closer to each other.

A comparison between the *E. coli* holocomplex model and interaction A in the R1E/R2F structure shows two, not too different situations. Docking of the R2F dimer to R1E into a position corresponding to R2 in the holocomplex model is done by a translation of just a few Ångströms followed by a rotation as shown in Figures 6.6b and 6.6c. This movement causes a displacement of about 30 Å in some parts of the R2F dimer. The movement have only minor effects on the distances between the radical carrying residues in any of the R2F monomers, and the active site of the R1E monomer mediating interaction A. The distances to the active site of the second R1E monomer however, decreases by approximately 20Å.

Loop 3 is clearly visible in the electron density maps in one of the R1E monomers in the asymmetric unit, the monomer not in contact with R2F in interaction A. When docking the R2F dimer to R1E forming a symmetrical holocomplex, similar to the *E. coli* model, loop 3 ends up in the interaction area between the subunits.

If interaction A is a preliminary state to the formation of a symmetrical holocomplex, binding of an R2F C-terminal peptide to the hydrophobic pocket of one R1E monomer is probably the initial and crucial contact between the two subunits. Depending of which of the R2F monomers in interaction A that bind to the R1E pocket, different conformations of the R2F C-termini will be obtained. If the R2F C-terminal peptide bound at the hydrophobic cleft of R1E monomer originates from the R2F monomer mediating interaction A, the C-terminus would be able to pass by the active site of R1E on its way to the hydrophobic pocket. The C-terminal tyrosine residue, Y304, would end up in the area in between W31 of R2F and Y693 of R1E in the symmetric holocomplex, able to act as a bridge between the subunits in the radical transfer chain. Assuming a rigid structure complex in interaction A, the distance to any of the radical transferring residues on either side of Y304, would however still be approximately 15Å.

In the second alternative, the peptide bound to the hydrophobic pocket is part of the R2F monomer that does not interact with R1E. A bridging Y304 between the two hydrogen bonded pathways in R2F and R1E is theoretically possible also in this case, but it seems less likely. The C-terminal tail would have to stretch from the position of the last traceable residue in R2F, 30 Å into the active site of R1E for positioning of Y304 between W31 on R2F and Y693 on R1E, and also folding back to the hydrophobic pocket. This way is far too long for the 33 amino acid residues missing in the C-terminus of this R2F monomer.

The conformational change of an R1E/R2F pair in interaction A, to a complex formation corresponding to the one in the *E. coli* model is not possible in the crystal packing. The movement would cause severe clashes between the subunits.

6.6 Conclusion

From the structure it is not possible to deduce if the observed relative positions of R1E and R2F in the crystal are the actual positions of the two homodimers in the biologically active complex, and how, in that case, the radical is transferred between the subunits.

The well defined electron density in the hydrophobic pocket of one of the R1E monomers in the asymmetric unit confirms the biological relevance of the cleft in R1E. Nothing else present in the crystallisation drop but a polypeptide could result in this kind of density. It is most likely that the observed interaction between the cleft in R1E and the suggested C-terminal polypeptide is the actual and crucial contact between the two subunits.

In the complex structure, each R1E interacts with two R2F subunits. The R2F being most likely to bind in the hydrophobic pocket of R1E is in contact with R1E through interaction A. Furthermore, the conserved residues of this R2F are pointing towards the active site of R1E.

The fact that only one hydrophobic cleft in R1E is occupied indicates that at least the initial contact between R1E and R2F is asymmetric. Whether this is the case also for the holocomplex in the moment of radical transfer is not possible to deduce from the structure.

6.7 Method

6.7.1 The beauty of Beast

The first crystals of the R1E/R2F complex were grown in 1997 and it was confirmed by SDS electrophoresis that they contained both subunits. One data set was collected to 6Å and the crystal belonged to one of the cubic space groups $p4_132$ or $p4_332$ with cell axes a=b=c=276Å (Eriksson,1997). A molecular replacement solution was identified but it was classified as questionable as a consequence of the low resolution.

In 2001 the crystallisation conditions were refined and a new data set to 4.5Å was collected. The new crystals turned out to be primitive tetragonal and not cubic as earlier even though they were grown with the same precipitant and buffer. The cell axes of the tetragonal crystals were a=b=276Å, c=270Å but missing reflections along the l-axis made it impossible to deduce the correct space group by the scaling statistics. Taking another look at the 6Å data it was discovered that even if refinement of the cell parameters indicated cubic symmetry there were systematic absences suggesting a tetragonal symmetry, $P4_32_12$ or $P4_12_12$. This result gave an indication that the new 4.5Å data might have 4/mmm point group symmetry with a slight change of the c axis.

Innumerable rotation trials with the 4.5Å tetragonal data scaled in P422 was run with the molecular replacement programs AmoRe (Navaza,1994), Molrep (Vagin

and Teplyakov,1997) and EPMR (Kissinger, et al.,1999). Unfortunately none of them was successful. Also, extensive trials using the same programs with the 6Å data set did not give any indication of a correct orientation, neither when the data was scaled cubically nor tetragonally. Because of its bigger size mainly the R1E homodimer was used as search model instead of R2F.

The first MR calculation that gave any solution was performed with the maximum likelihood based program Beast (Read,2001). It was a search with R1E in the 6Å dataset scaled in the cubic space group $P4_132$, that finally generated a clear solution. There was one R1E dimer per asymmetric unit (au) and the generation of symmetry related subunits demonstrated good crystal contacts and room for one R2F in each asymmetric unit.

While attempts were made to transfer the cubic solution to the tetragonal cell, Beast was employed on the higher resolution dataset scaled in $P4_12_12$, a non-isomorphic subgroup to $P4_132$. Six rotation solutions were identified and eventually also two translation solutions searching with the R1E dimer. Since the translation search turned out to be very time-consuming, one week for one eighth of the Cheshire cell, the third and last R1E dimer was positioned manually by comparing with the cubic MR solution. The three R2F dimers were placed by hand in the electron density maps.

Subsequent data collections on different crystals obtained under similar crystallisation conditions show mainly tetragonal symmetry. However, the best diffracting crystal belongs to the cubic space group $P4_132$ with cell parameters a=b=c=270Å. As in the original crystals, the symmetry is cubic, but the unit cell is slightly smaller. The crystals contain one R1E dimer and one R2F dimer per asymmetric unit, and have a solvent content of 66%.

6.7.2 Transmission Electron Microscopy

In addition to the crystallographic investigations of the *S. typhimurium* R1E/R2F holocomplex, attempts were made to use transmission electron microscopy for characterisation of the complex. 1% tungsten-phosphoric acid was used as a negative stain. Unfortunately the protein complex turned out to be too small to be visualised by this method. The proteins could also have been denatured, or in some other way affected, by the negative stain.

The electron microscopy work was done in collaboration with Hans Hebert at the Department of Biosciences, Karolinska Institutet in Stockholm.

References

Andersson, M. E., Högbom, M., Rinaldo-Matthis, A., Andersson, K. K., Sjöberg, B.-M. and Nordlund, P. (1999) The crystal structure of an azide complex of the diferrous R2 subunit of ribonucleotide reductase displays a novel carboxylate shift with important mechanistic implications for diiron-catalyzed oxygen activation. *J Am Chem Soc,* **121,** 2346-2352.

Assarsson, M., Andersson, M. E., Högbom, M., Persson, B. O., Sahlin, M., Barra, A. L., Sjöberg, B. M., Nordlund, P. and Gräslund, A. (2001) Restoring proper radical generation by azide binding to the iron site of the E238A mutant R2 protein of ribonucleotide reductase from *Escherichia coli*. *J Biol Chem,* **276,** 26852-9.

Becker, A., Fritz-Wolf, K., Kabsch, W., Knappe, J., Schultz, S. and Volker Wagner, A. F. (1999) Structure and mechanism of the glycyl radical enzyme pyruvate formate-lyase. *Nat Struct Biol,* **6,** 969-75.

Bergfors, T. M. (1999) *Protein Crystallization - Techniques, Strategies, and Tips,* International University Line, La Jolla.

Brown, N. C., Canellakis, Z. N., Lundin, B., Reichard, P. and Thelander, L. (1969) Ribonucleoside diphosphate reductase. Purification of the two subunits, proteins B1 and B2. *Eur J Biochem,* **9,** 561-73.

Brown, N. C. and Reichard, P. (1969a) Ribonucleoside diphosphate reductase. Formation of active and inactive omplexes if proteins B1 and B2. *J Mol Biol,* **46,** 25-38.

Brown, N. C. and Reichard, P. (1969b) Role of Effector Binding in Allosteric Colntrol of Ribonucleoside Diphosphate Reductaes. *J Mol Biol,* **46,** 39-55.

Climent, I., Sjöberg, B. M. and Huang, C. Y. (1991) Carboxyl-terminal peptides as probes for Escherichia coli ribonucleotide reductase subunit interaction: kinetic analysis of inhibition studies. *Biochemistry,* **30,** 5164-71.

Climent, I., Sjöberg, B. M. and Huang, C. Y. (1992) Site-directed mutagenesis and deletion of the carboxyl terminus of *Escherichia coli* ribonucleotide reductase protein R2. Effects on catalytic activity and subunit interaction. *Biochemistry,* **31,** 4801-7.

Cohen, E. A., Gaudreau, P., Brazeau, P. and Langlier, Y. (1986) Specific inhibition of herpes virus ribonucleotide reductase by a nonapeptide derived from the carboxy terminus of subunit 2. *Nature,* **321,** 441-442.

Cosentino, G., Lavallee, P., Rakhit, S., Plante, R., Gaudette, Y., Lawetz, C., Whitehead, P. W., Duceppe, J.-S., Lepine-Frenette, C., Dansereau, N., Gilbault, C., Langlier, Y., Gaudreau, P., Thelander, L. and Guindon, Y. (1991) Specific inhibition of ribonucleotide reductase by peptides corresponding to the C-terminal of their second subunit. *Biochem Cell Biol,* **69,** 79-83.

Dutia, B. M., Frame, M. C., Subak-Sharpe, J. H., Clark, W. N. and Marsden, H. S. (1986) Specific inhibition of herpesvirus ribonucleotide reductase by synthetic peptides. *Nature,* **321,** 439-441.

Ehrenberg, A. and Reichard, P. (1972) Electron spin resonance of the iron-containing protein B2 from ribonucleotide reductase. *J Biol Chem,* **247,** 3485-3488.

Ekberg, M., Pötsch, S., Sandin, E., Thunnissen, M., Nordlund, P., Sahlin, M. and Sjöberg, B. M. (1998) Preserved catalytic activity in an engineered ribonucleotide reductase R2 protein with a nonphysiological radical transfer pathway. The importance of hydrogen bond connections between the participating residues. *J Biol Chem,* **273,** 21003-8.

Ekberg, M., Sahlin, M., Eriksson, M. and Sjöberg, B. M. (1996) Two conserved tyrosine residues in protein R1 participate in an intermolecular electron transfer in ribonucleotide reductase. *J Biol Chem,* **271,** 20655-9.

Eklund, H. and Fontecave, M. (1999) Glycyl radical enzymes: a conservative structural basis for radicals. *Structure Fold Des,* **7,** R257-62.

Eklund, H., Uhlin, U., Färnegårdh, M., Logan, D. T. and Nordlund, P. (2001) Structure and function of the radical enzyme ribonucleotide reductase. *Prog Bioph Mol Biol,* **77,** 177-268.

Eliasson, R., Pontis, E., Jordan, A. and Reichard, P. (1996) Allosteric regulation of the third ribonucleotide reductase (NrdEF enzyme) from enterobacteriaceae. *J Biol Chem,* **271,** 26582-26587.

Eriksson, M. (1997) In *Department of Molecular Biology*Swedish University of Agricultural Sciences, Uppsala.

Eriksson, M., Jordan, A. and Eklund, H. (1998) Structure of *Salmonella typhimurium* nrdF Ribonucleotide Reductase in its oxidized and reduced form. *Biochemistry,* **37,** 13359-13369.

Eriksson, M., Uhlin, U., Ramaswamy, S., Ekberg, M., Regnström, K., Sjöberg, B. M. and Eklund, H. (1997) Binding of allosteric effectors to ribonucleotide reductase protein R1: reduction of active-site cysteines promotes substrate binding. *Structure,* **5,** 1077-92.

Fraser, C. M., J. D. Gocayne, O. White, M. D. Adams, R. A. Clayton, R. D. Fleischmann, C. J. Bult, A. R. Kerlavagne, G. Sutton, J. M. Kelley, J. L. Fritchman, J. F. Weidman, K. V. Small, M. Sandusky, J. Fuhrmann, D. Nguyen, T. R. Utterback, D. M. Saudek, and Venter., J. C. (1995) The minimal gene complement of *Mycoplasma genitalium*. *Science,* **270,** 397-403.

Ge, J., Yu, G. X., Ator, M. A. and Stubbe, J. (2003) Pre-steady-state and steady-state kinetic analysis of *E. coli* class I ribonucleotide reductase. *Biochemistry,* **42,** 10071-10083.

Holmgren, A. (1989) Thioredoxin and glutaredoxin systems. *J Biol Chem,* **264,** 13963-13966.

Huque, Y. (2001) In *Department of Molecular Biology and Functional Genomics,*Stockholm University, Stockholm.

Högbom, M., Andersson, M. E. and Nordlund, P. (2001) Crystal structures of oxidized dinuclear manganese centres in Mn-substituted class I ribonucleotide reductase from *Escherichia coli*: carboxylate shifts with implications for O2 activation and radical generation. *J Biol Inorg Chem,* **6,** 315-23.

Högbom, M., Galander, M., Andersson, M., Kolberg, M., Hofbauer, W., Lassmann, G., Nordlund, P. and Lendzian, F. (2003) Displacement of the

tyrosyl radical cofactor in ribonucleotide reductase obtained by single-crystal high-field EPR and 1.4-A x-ray data. *Proc Natl Acad Sci U S A,* **100,** 3209-14.

Högbom, M., Huque, Y., Sjöberg, B. M. and Nordlund, P. (2002) Crystal structure of the di-iron/radical protein of ribonucleotide reductase from *Corynebacterium ammoniagenes*. *Biochemistry,* **41,** 1381-9.

Högbom, M., Stenmark, P., McClarty, G. and Nordlund, P. (2004) The Chlamydia ribonucleotide reductase - a novel radical site in Class-I R2s. *Manuscript*.

Jordan, A., Aragall, E., Gibert, I. and Barbe, J. (1996a) Promoter identification and expression analysis of *Salmonella typhimurium* and *Escherichia coli* nrdEF operons encoding one of two class I ribonucleotide reductases present in both bacteria. *Mol Microbiol,* **19,** 777-790.

Jordan, A., Gibert, I. and Barbe, J. (1994a) Cloning and sequencing of the genes from *Salmonella typhimurium* encoding a new bacterial ribonucleotide reductase. *J Bacteriol,* **176,** 3420-3427.

Jordan, A., Pontis, E., Atta, M., Krook, M., Gibert, I., Barbe, J. and Reichard, P. (1994b) A second class I ribonucleotide reductase in Enterobacteriaceae: Characterization of the *Salmonella typhimurium* enzyme. *Proc Natl Acad Sci USA,* **91,** 12892-12896.

Jordan, A., Pontis, E., Åslund, F., Hellman, U., Gibert, I. and Reichard, P. (1996b) The ribonucleotide reductase system of *Lactococcus lactis* - Characterization of an nrdEF enzyme and a new electron transport protein. *J Biol Chem,* **271,** 8779-8785.

Jordan, A. and Reichard, P. (1998) Ribonuclotide reductases. *Ann Rev Biochem,* **67,** 71-98.

Jordan, A., Åslund, F., Pontis, E., Reichard, P. and Holmgren, A. (1997) Characterization of Escherichia coli NrdH - A glutaredoxin-like protein with a thioredoxin-like activity profile. *J Biol Chem,* **272,** 18044-18050.

Kashlan, O. B., Scott, C. P., Lear, J. D. and Cooperman, B. S. (2002) A comprehensive model for the allosteric regulation of mammalian ribonucleotide reductase. Functional consequences of ATP- and dATP-induced oligomerization of the large subunit. *Biochemistry,* **41,** 462-74.

Kauppi, B., Nielsen, B. B., Ramaswamy, S., Larsen, I. K., Thelander, M., Thelander, L. and Eklund, H. (1996) The three-dimensional structure of mammalian ribonucleotide reductase protein R2 reveals a more-accessible iron-radical site than *Escherichia coli* R2. *J Mol Biol,* **262,** 706-20.

Kissinger, C. R., Gehlhaar, D. K. and Fogel, D. B. (1999) Rapid automated molecular replacement by evolutionary search. *Acta Cryst D,* **55 (Pt 2),** 484-91.

Kunz, B. A. (1988) Mutagenesis and deoxyribonucleotide pool imbalance. *Mutat Res,* **200,** 133-147.

Larsson, A., Karlsson, M., Sahlin, M. and Sjöberg, B. M. (1988) Radical formation in the dimeric small subunit of ribonucleotide reductase requires only one tyrosine 122. *J Biol Chem,* **263,** 17780-4.

Larsson, A. and Sjöberg, B. M. (1986) Identification of the stable free radical tyrosine residue in ribonucleotide reductase. *Embo J,* **5,** 2037-40.

Larsson, K. M., Andersson, J., Sjoberg, B. M., Nordlund, P. and Logan, D. T. (2001) Structural basis for allosteric substrate specificity regulation in anaerobic ribonucleotide reductases. *Structure (Camb),* **9,** 739-50.

Licht, S., Gerfen, G. J. and Stubbe, J. (1996) Thiyl radicals in ribonucleotide reductases. *Science,* **271,** 477-481.

Liu, A., Potsch, S., Davydov, A., Barra, A. L., Rubin, H. and Gräslund, A. (1998) The tyrosyl free radical of recombinant ribonucleotide reductase from *Mycobacterium tuberculosis* is located in a rigid hydrophobic pocket. *Biochemistry,* **37,** 16369-77.

Logan, D. T., Andersson, J., Sjöberg, B. M. and Nordlund, P. (1999) A glycyl radical site in the crystal structure of a class III ribonucleotide reductase. *Science,* **283,** 1499-504.

Logan, D. T., Su, X. D., Åberg, A., Regnström, K., Hajdu, J., Eklund, H. and Nordlund, P. (1996) Crystal structure of reduced protein R2 of ribonucleotide reductase: the structural basis for oxygen activation at a dinuclear iron site. *Structure,* **4,** 1053-64.

Mao, S. S., Holler, T. P., Bollinger, J. M., Jr., Yu, G. X., Johnston, M. I. and Stubbe, J. (1992a) Interaction of C225SR1 mutant subunit of ribonucleotide reductase with R2 and nucleoside diphosphates: Tales of a suicidal enzyme. *Biochemistry,* **31,** 9744-9751.

Mao, S. S., Yu, G. X., Chalfoun, D. and Stubbe, J. (1992b) Characterization of C439SR1, a Mutant of *Escherichia coli* Ribonucleotide Diphosphate Reductase: Evidence That C439 Is a Residue Essential for Nucleotide Reduction and C439SR1 Is a protein Possessing Novel Thioredoxin-like Activity. *Biochemistry,* **31,** 9752-9759.

Navaza, J. (1994) AMoRe: an Automated Package for Molecular Replacement. *Acta Cryst A,* **50,** 157-163.

Nordlund, P., Sjöberg, B. M. and Eklund, H. (1990) Three-dimensional structure of the free radical protein of ribonucleotide reductase. *Nature,* **345,** 593-8.

Persson, B. O., Karlsson, M., Climent, I., Ling, J. S., Loehr, J. S., Sahlin, M. and Sjöberg, B. M. (1996) Iron ligand mutants in protein R2 of *Escherichia coli* ribonucleotide reductase - Retention of diiron site, tyrosyl radical and enzymatic activity in mutant proteins lacking an iron-binding side chain. *J Biol Inorg Chem,* **1,** 247-256.

Read, R. J. (2001) Pushing the boundaries of molecular replacement with maximum likelihood. *Acta Cryst D,* **57,** 1373-1382.

Reichard, P. (1993) From RNA to DNA, why so many ribonucleotide reductases? *Science,* **260,** 1773-1777.

Reichard, P. (1997) The evolution of ribonucleotide reduction. *TIBS,* **22,** 81-85.

Reichard, P. and Ehrenberg, A. (1983) Ribonucleotide reductase - a radical enzyme. *Science,* **221,** 514-519.

Reichard, P. and Rutberg, L. (1960) Formation of deoxycytidine 5'-phosphate from cytidine 5'-phosphate with enzymes from *Escherichia coli*. *Biochem Biophys Acta,* **37,** 554-5.

Rova, U., Adrait, A., Potsch, S., Gräslund, A. and Thelander, L. (1999) Evidence by mutagenesis that Tyr(370) of the mouse ribonucleotide reductase R2 protein is the connecting link in the intersubunit radical transfer pathway. *J Biol Chem,* **274,** 23746-51.

Rova, U., Goodtzova, K., Ingemarson, R., Behravan, G., Gräslund, A. and Thelander, L. (1995) Evidence by site-directed mutagenesis supports long-range electron transfer in mouse ribonucleotide reductase. *Biochemistry,* **34,** 4267-75.

Sahlin, M., Sjöberg, B.-M., Backes, G., Loehr, T. and Sanders-Loehr, J. (1990) Activation of the iron-containing B2 protein of ribonucleotide reductase by hydrogen peroxide. *Biochem Biophys Res Comm,* **167,** 813-818.

Scott, C. P., Kashlan, O. B., Lear, J. D. and Cooperman, B. S. (2001) A quantitative model for allosteric control of purine reduction by murine ribonucleotide reductase. *Biochemistry,* **40,** 1651-61.

Scotti, C., Valbuzzi, A., Perego, M., Galizzi, A. and Albertini, A. M. (1996) The *Bacillus subtilis* genes for ribonucleotide reductase are similar to the genes for the second class I NrdE/NrdF enzymes of Enterobacteriaceae. *Microbiol Uk,* **142,** 2995-3004.

Siegbahn, E. M. (2003) Mechanisms of metalloenzymes studied by quantum chemical methods. *Quart Rev Bioph,* **36,** 91-145.

Siegbahn, P. E. M., Eriksson, L., Himo, F. and Pavlov, M. (1998) Hydrogen atom transfer in ribonucleotide reductase (RNR). *J Phys Chem B,* **102,** 10622-10629.

Sintchak, M. D., Arjara, G., Kellogg, B. A., Stubbe, J. and Drennan, C. L. (2002) The crystal structure of class II ribonucleotide reductase reveals how an allosterically regulated monomer mimics a dimer. *Nat Struct Biol,* **9,** 293-300.

Sjöberg, B. M. (1994) The ribonucleotide reductase jigsaw puzzle: a large piece falls into place. *Structure,* **2,** 793-6.

Sjöberg, B. M. (1997) Ribonucleotide reductases - A group of enzymes with different metallosites and a similar reaction mechanism. *Structure and Bonding,* **88,** 139-173.

Sjöberg, B. M. and Gräslund, A. (1977) The free radical in ribonucleotide reductase from *E. coli*. *Ciba Found Symp,* **252,** 187-96.

Sjöberg, B. M., Karlsson, M. and Jörnvall, H. (1987) Half-site reactivity of the tyrosyl radical of ribonucleotide reductase from *Escherichia coli*. *J Biol Chem,* **262,** 9736-43.

Sjöberg, B. M. and Reichard, P. (1977) Nature of the free radical in ribonucleotide reductase from Escherichia coli. *J Biol Chem,* **252,** 536-41.

Stehr, M., Schneider, G., Åslund, F., Holmgren, A. and Lindqvist, Y. (2001) Structural basis for the thioredoxin-like activity profile of the glutaredoxin-like NrdH-redoxin from *Escherichia coli*. *J Biol Chem,* **276,** 35836-35841.

Stubbe, J. (2000) Ribonucleotide reductases: the link between an RNA and a DNA world? *Curr Opin Struct Biol,* **10,** 731-6.

Stubbe, J. (2003) Di-iron-tyrosyl radical ribonucleotide reductases. *Curr Op Chem Biol,* **7,** 183-188.

Stubbe, J., Ge, J. and Yee, C. S. (2001) The evolution of ribonucleotide reduction revisited. *Trends Biochem Sci,* **26,** 93-9.

Stubbe, J., Nocera, D. G., Yee, C. S. and Chang, M. C. (2003) Radical initiation in the class I ribonucleotide reductase: long-range proton-coupled electron transfer? *Chem Rev,* **103,** 2167-201.

Stubbe, J. and van der Donk, W. A. (1998) Protein radicals in enzyme catalysis. *Chem rev,* **98,** 705-762.

Thelander, L. (1973) Physicochemical characterization of ribonucleoside diphosphate reductase from Escherichia coli. *J Biol Chem,* **248,** 4591-601.

Thelander, L. and Reichard, P. (1979) Reduction of ribonucleotides. *Annu Rev Biochem,* **48,** 133-58.

Torrents, E., Aloy, P., Gibert, I. and Rodriguez-Trelles, F. (2002) Ribonucleotide reductases: divergent evolution of an ancient enzyme. *J Mol Evol,* **55,** 138-52.

Uhlin, U. and Eklund, H. (1994) Structure of ribonucleotide reductase protein R1. *Nature,* **370,** 533-539.

Uppsten, M., Färnegårdh, M., Jordan, A., Eliasson, R., Eklund, H. and Uhlin, U. (2003) Structure of the large subunit of class Ib ribonucleotide reductase from *Salmonella typhimurium* and its complexes with allosteric effectors. *J Mol Biol,* **330,** 87-97.

Vagin, A. and Teplyakov, A. (1997) MOLREP: an automated program for molecular replacement. *J App Cryst,* **30,** 1022-1025.

WHO (2003) *Global Tuberculosis control, Surveillance, Planning, Financing*, Geneva.

Voegtli, W. C., Ge, J., Perlstein, D. L., Stubbe, J. and Rosenzweig, A. C. (2001) Structure of the yeast ribonucleotide reductase Y2Y4 heterodimer. *Proc Natl Acad Sci U S A,* **98,** 10073-8.

Yang, F. D., Curran, S. C., Li, L. S., Avarbock, D., Graf, J. D., Chua, M. M., Lui, G. Z., Salem, J. and Rubin, H. (1997) Characterization of two genes encoding the *Mycobacterium tuberculosis* ribonucleotide reductase small subunit. *J Bacteriol,* **179,** 6408-6415.

Yang, F. D., Lu, G. Z. and Rubin, H. (1994) Isolation of ribonucleotide reductase from *Mycobacterium tuberculosis* and cloning, expression, and purification of the large subunit. *J Bacteriol,* **176,** 6738-6743.

Åberg, A., Hahne, S., Karlsson, M., Larsson, A., Ormö, M., Ahgren, A. and Sjöberg, B. M. (1989) Evidence for two different classes of redox-active cysteines in ribonucleotide reductase of *Escherichia coli*. *J Biol Chem,* **264,** 12249-52.

Thank you!

First of all, my supervisor **Ulla**, thank you for everything! For your care, encouragement, magic crystallisation fingers and for our enthusiastic discussions about the holocomplex. I really enjoyed working with you!

Hasse, your are a cool "dalmas" with truly impressive knowledge about science. Thank you for the interesting discussions as well as the relaxed lunches at Hammarskog!

I would like to express my gratitude to **Hans Hebert** at the Department of Biosciences at Karolinska Institutet for a good collaboration with the RNR holocomplex. I would also like to thank **Janos** for providing the microspectophotometer and **Gunilla** for invaluable instructions.

Rosie, thank you for sharing everything the last 4.5 years! Thanks for all the fun and for always listening. I will miss having you behind my back every day!

Andreas Smartass! Thank you for sharing many thoughts, all the support and crazy discussions!

Urszula (professor Kosinska), thanks for the talks, the Polish-lessons, the skiing and more. You will be the best of professors one day (if you would like..)!

Fredrik, slime-darling! Thank you for your help at times when I needed it!

Andrea, slime darling2! You impress me with your love for slime and complicated gels. Good luck!

Martin, thanks for the fun teaching and for always being so positive!

Double Doctor **Deva**, you were my guide into the world of Linux and a lot of the other strange stuff I ran into when I started my PhD. Thank you for your help and friendship!

Mark, I have many heroes but you are a truly special one! Thank you for all your help during the years AND the ice skating!! Good luck with your house!

Vladimir I miss you and your enthusiasm! Thank you for sharing your love for science!

Christer, Erling and **David** – my heroes! Thank you for all your endless support in the frustrating world of computers.

Nisse, thanks for help with my troublesome computers. I would not have made it without you help!

Rams, you have enough energy for the whole of Uppsala and Iowa. Thank you for sharing some, and letting me stay in you lab in Iowa for 3 weeks!

Margareta and **Elleonor** thank you for cat-support and help with paper work and order in the lab.

Linda, Karin, Jenny, Emma -You are the coolest of ladies! Thanks for all the laughs!

Al, Saeid, Linda, Karin, Rosie, Urszula, Susanna, Jenny – Thank you for making the synchrotron trips so much fun!

Emma, Louise, , Inés, Evalena, Lars, Kenth, Stefan, Jerry, Anton, Inger, Janos, Tom, Anke, Remco, Ulrika, Patrik, Jimmy, Gunilla, Annette, Lena, Alina, Alexandra, Sara, Talal, Seved, Tex, Totte, Isabella, Nina, Gunnar, Ola, Mats, Martin, Martin, Martin, Martin, Martin osv…. Thank you **all@xray** for making it so great to work here!

Börje, tack för ditt förtroende, din hjärtliga omsorg och tack för fantastiska diskussioner! Jag hoppas vi ses snart!

Världens bästa vänner, jag är tacksam för att ni stöttat mig dessa år, och låtit mig vara ofantligt tråkig de senaste månaderna! **Johanna**, tack för din aldrig sinande entusiasm och glädje! Du gör mig så glad! **Mari,** Du ger mig perspektiv på forskartillvaron och får mig att se vad som verkligen betyder någonting! Tack! Min **Anna**, själsfrände. Vi tystnar aldrig! **Berit** och **Peter**, tack för ert fantastiska stöd i början av min forskarkarriär! Min kära **Malin**, jag saknar fortfarande att inte ha dig på armlängds avstånd. **Ulle**, du är sååå bra som alltid kan lyssna och förstå, inte bara science problem.

Mamma, Pappa och **Martin** ni är dom bästa som finns!

Niclas min kärlek! Tack för all glädje och kärlek Du ger mig alla dagar!

Appendix A

Data collection and refinement statistics on the structure of *S. typhimurium* R1E in complex with its allosteric specificity effector dGTP.

Beamline	ESRF, ID14-4
Wavelength (Å)	0.9340
Cell parameters (Å, deg)	99, 99, 288, 90, 90, 90
Space group	$p4_32_12$
Resolution range (Å)	40-3.0
Redundancy	6.2
R_{merge} [a]	9.6 (45.1)
I/σ (I)	14.3 (3.6)
Completeness (%)	99.8 (100.0)
No. observations	186822
No. unique reflections	30116
R_{cryst} [b]	0.26
R_{free} [c]	0.29
r.m.s.d. bond lengths (Å)	0.02
r.m.s.d. angle (deg.)	1.71
Average *B*-factor (Å^2)	34.8

Numbers in parentheses refer to the highest resolution shell.

[a] $R_{merge} = (\Sigma_{hkl}\Sigma_i |I_i(hkl) - \langle I(hkl)\rangle| / \Sigma_{hkl}\Sigma_i I_i(hkl)$ x 100 % for n independent reflections and i observations of a given reflection. $\langle I(hkl)\rangle$ is the average intensity of the I observation.

[b] $R_{cryst} = \Sigma_h ||F_o(h)| - |F_c(h)|| / \Sigma_h |F_o(h)|$, where F_o and F_c are the observed and calculated structure factors respectively.

[c] R_{free} is equivalent to F_{cryst} for a 5% subset of reflections not used in the refinement.